PlanetCam UPV/EHU: A two channel lucky imaging camera for Solar System studies in the spectral range 0.38 – 1.7 μm

IÑIGO MENDIKOA[1], AGUSTÍN SÁNCHEZ-LAVEGA[1-2], SANTIAGO PÉREZ-HOYOS[1-2], RICARDO HUESO[1-2], JOSÉ FÉLIX ROJAS[1-2], JESÚS ACEITUNO[3-4], FRANCISCO ACEITUNO[5], GAIZKA MURGA[6], LANDER DE BILBAO[6], AND ENRIQUE GARCÍA-MELENDO[1-7]

ABSTRACT We present PlanetCam UPV/EHU, an astronomical camera designed fundamentally for high-resolution imaging of Solar System planets using the "lucky imaging" technique. The camera observes in a wavelength range from 380 nm to 1.7 μm and the driving science themes are atmosphere dynamics and vertical cloud structure of Solar System planets. The design comprises two configurations that include one channel (visible wavelengths) for high magnification or two combined channels (visible and short wave infrared) working simultaneously at selected wavelengths by means of a dichroic beam splitter (Sanchez-Lavega et al., 2012). In this paper the camera components for the two configurations are described, as well as camera performance and the different tests done for the precise characterization of its radiometric and astrometric capabilities at high spatial resolution. Finally, some images of solar system objects are presented as well as photometric results and different scientific cases on astronomical targets.

[1] Departamento de Física Aplicada I, E.T.S. Ingeniería, Universidad del País Vasco, Alameda Urquijo s/n, 48013 Bilbao. Spain.
[2] Unidad Asociada Grupo Ciencias Planetarias UPV/EHU- IAA (CSIC). Spain.
[3] Centro Astronómico Hispano Alemán, Calar Alto, (CSIC-MPG), Sierra de los Filabres, 04550 Gergal, Spain.
[4] iTec-Astronomica, c/Albacete 2, El Puerto de Santa María, Cádiz, Spain.
[5] Instituto de Astrofísica de Andalucía, Glorieta de la Astronomia s/n, 18008 Granada. Spain.
[6] IDOM, Av. Zarandoa Etorbidea, 23, 48015 Bilbao, Spain.
[7] Fundació Observatori Esteve Duran, Montseny 46, 08553 Seva, Barcelona. Spain.

1. INTRODUCTION

Imaging astronomical objects at high spatial resolution requires overcoming the pernicious effects of atmospheric turbulence generically known as "seeing" in the astronomical context (Fried, 1965). The use of space telescopes and active and adaptive optical systems have been the classical solutions (Hardy J.W., 2000). With a lower cost, the "lucky imaging technique" based on the alignment and stacking of hundreds or thousands of short exposures (Lelièvre et al., 1988; Law et al., 2005), has been successfully employed for high resolution at visible wavelengths in a number of astronomical contexts. Among others, the lucky-imaging technique has become popular in the amateur world (Mousis et al., 2014) allowing astronomical images acquired by amateurs operating small-size telescopes to be successfully used in planetary atmospheres research (Sánchez-Lavega et al., 2008, 2010, 2011, 2015; Barrado-Izagirre et al., 2013). There are a number of astronomical cameras based on the lucky imaging concept operating in different observatories, all of them at visible wavelengths. One of the earliest was *LuckyCam* developed at the Cambridge University (Law, 2006) used at the Nordic Optical Telescope in Roque de los Muchachos (La Palma, Canarias, Spain) (http://www.not.iac.es/instruments/luckycam/) and also at the 200-inches Hale telescope in Mount Palomar Observatory (http://www.astro.caltech.edu/~nlaw/lucky_palomar/). The lucky-imaging concept was also used by the camera *AstraLux*, developed by the Max Planck Institute for Astronomy (Hormuth, 2007). *AstraLux* is used at Calar Alto Observatory (Almeria, Spain – AstraLux Norte) and on La Silla Observatory (Chile – AstraLux Sur). *FastCam* is another example, designed by the Instituto de Astrofisica de Canarias and Universidad Politécnica de Cartagena (López-López, 2012).

In this paper *PlanetCam UPV/EHU* (hereafter *PlanetCam*) is described, an astronomical camera designed for the observation of planetary atmospheres at high spatial resolution simultaneously in two channels: visible (0.38 – 1 μm) and short wave near infrared SWIR (1 – 1.7

μm) (Sánchez-Lavega et al., 2012). It consists of two arms or channels, each one with its own detector and filters of interest for planetary atmospheres research. This paper deals with the description and performances of *PlanetCam* for the study of solar system objects. The main objective of *PlanetCam* is the study, on a regular basis, at various spatial and temporal scales of the atmospheres of Venus, Mars, Jupiter, Saturn, Uranus, Neptune and the satellite Titan. This comprises the evolution of the vertical distribution and properties of clouds and hazes, retrieval of atmospheric winds in Jupiter, Saturn and Venus, the study of their meteorological phenomena, and the study of occasional events such as transient major atmospheric disturbances (Sánchez-Lavega et al., 1982, 2008, 2011, 2015), impacts on Jupiter (Sánchez-Lavega et al., 2010; Hammel et al., 2010; Hueso et al., 2010, 2013) or atmospheric features in Mars (Sánchez-Lavega et al. 2014). Other Solar System objects are also potential targets for *PlanetCam*, particularly when high spatial or temporal resolution are required, such as activity in comets, asteroids, and occultation phenomena that require a high rate temporal sampling. *PlanetCam* has been also tested and occasionally used for a fast response to the detection of a Gamma Ray Burst (Gorosabel et al., 2013) and extrasolar planet transits. Finally, other potential astronomical targets for the camera are binary and multiple stellar systems, and globular clusters.

PlanetCam has been designed for two possible operational independent configurations: *PlanetCam1* is aimed to perform observations only in the visible channel (380 nm – 1μm), and *PlanetCam2* provides simultaneous observations in visible (using the same detector as in configuration 1) and the SWIR (1 – 1.7 μm) (Sánchez-Lavega et al., 2012). *PlanetCam1* is easily transportable and has been tested in a variety of telescopes. The first tests on *PlanetCam1* were performed on the 0.5 m telescope at the Observatorio Aula Espazio Gela in the University of the Basque Country in 2012 (Sánchez-Lavega et al., 2014). The regular scientific use of *PlanetCam* has been performed at the 1.23 m and 2.2 m telescopes of the Centro Astronómico Hispano-Alemán (CAHA) at Calar Alto Observatory (Almería, Spain). Some tests have been run also at the 1.05 m telescope at Pic du Midi Observatory (France), as well as the 1.5 m Telescopio Carlos Sánchez (TCS) at Teide Observatory pertaining to the Instituto de Astrofísica de Canarias (IAC). *PlanetCam2* is a more complex instrument and currently operates only at the 1.23 and 2.2m telescopes at Calar Alto Observatory in Spain. This paper describes the instrument for each configuration and the laboratory tests and performances on astronomical observations.

The organization of this paper is as follows. In section 2 the *PlanetCam* concept is described for the two configurations of the camera. Section 3 is devoted to the characterization of the visible channel and its sCMOS detector while section 4 describes the SWIR channel and its InGaAs detector. Sections 5 and 6 deal with the camera control and shortly describe the image processing methods. The astronomical performance of *PlanetCam* is presented in section 7, presenting section 8 some examples of planetary images and section 9 those for different astronomical targets.

2. GENERAL INSTRUMENT DESCRIPTION

The *PlanetCam* concept includes two operational independent configurations. *PlanetCam1* is a low weight and easily transportable and manageable camera for a fast installation in a telescope when a quick observational response is needed if an unusual or unexpected event occurs. It can be mounted in small telescopes (diameters ≥ 0.5m) and provides different magnifications employing a system of interchangeable Barlow lenses. *PlanetCam2* is a more complex and heavier instrument with two channels that operate simultaneously and require independent operation and control.

2.1 Configuration of PlanetCam1

Under the first configuration, *PlanetCam1* operates only in the visible channel and with a high magnification at the focal plane. The main elements constituting the camera are a sCMOS detector (also employed in *PlanetCam2* visible channel), two filter wheels and an interchangeable Barlow lens to provide the required magnification (Figure 1, Sánchez-Lavega et al., 2012).

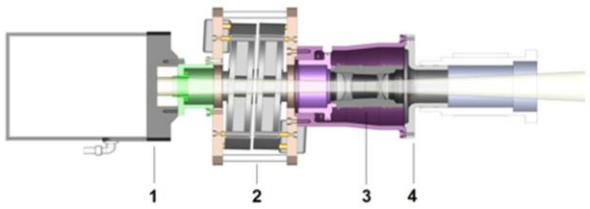

FIG. 1.- *PlanetCam1* engineering diagram showing from left to right: 1-sCMOS detector, 2-filter wheels, 3-Barlow lens and 4-telescope adaptor. Quick access to the Barlow lens is possible by removing one lid in the lateral structure supporting the instrument. The inclination of the filters wheels avoids internal reflections.

2.2 Configuration of PlanetCam2

This mode has two channels (visible and SWIR) operating simultaneously. A scheme of the instrument and its location at the telescope focus is shown in Figure 2, while Figure 3 shows the optical configuration of the camera. The beam from the telescope is first collimated and then split at 90° in two beams (visible and SWIR wavelengths) by the dichroic element. Before reaching the detector, the beam in each channel passes through a filter wheel for selection of the spectral range and an optical magnification system (three possible magnifications are available). Motorized modules are used on each channel for selection of one over three possible optical configurations. Each configuration requires focusing the camera by changing the position of the detector with respect to the focus of the telescope, which remains the same to obtain a collimated beam before the dichroic splitter. Focusing of each detector is achieved by a motorized automatic stage.

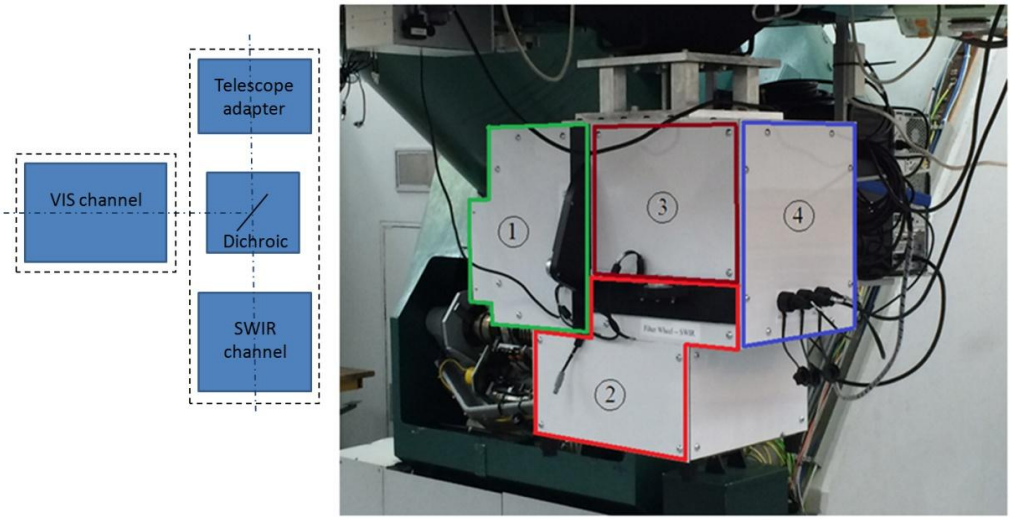

FIG. 2.- Left: *PlanetCam2* general scheme. Right: *PlanetCam2* attached to the Cassegrain focus of the 1.23m of Calar Alto Observatory. Each subsystem module has been colored in the picture: (1) Visible channel, (2) SWIR channel, (3) Collimator and dichroic, (4) Electronics.

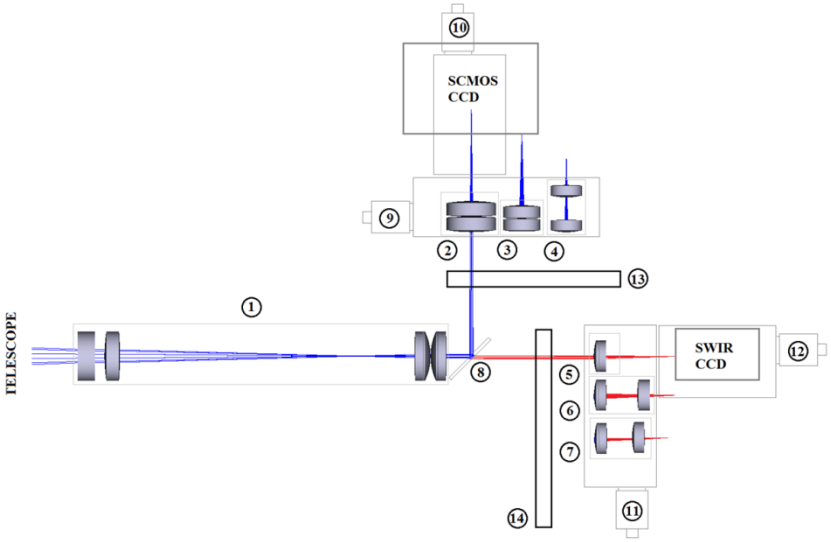

FIG. 3.- *PlanetCam2* diagram showing the following elements:(1) Collimator, (2-4) Optical magnification for the visible channel (high, medium, low), (5-7) Optical magnification for the SWIR channel (high, medium, low), (8) beam splitter, (9) motorized linear stage for visible scale selection, (10) motorized linear stage for focusing the visible arm, (11) motorized linear stage for SWIR scale selection, (12) motorized linear stage for focusing the SWIR arm, (13) visible filter wheel, (14) SWIR filter wheel.

2.2.1 Collimation of the telescope beam

In order to avoid optical distortion in the transmitted optical path, the light beam from the telescope is first collimated before arriving the dichroic. A collimator based on commercial lenses has been designed as shown in Figure 4. It combines a Kepler and Galileo telescopes scheme with the lenses properties given in Table 1. The design is optimized for the camera operation in the whole spectral range (350 – 1,700 nm). Figure 5 shows the transmission efficiency of the collimating system as provided by the manufacturer.

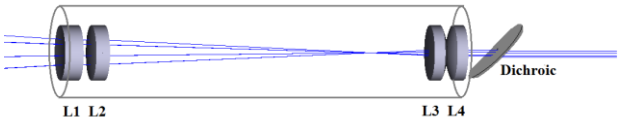

FIG. 4.- Ray diagram for the collimating optical system in *PlanetCam2*.

Table 1

LENSES EMPLOYED IN THE COLLIMATING SYSTEM OF PLANETCAM2

Lens	Diameter (mm)	Focal Length (mm)	Coating
L1	40	-150	MgF_2
L2	40	200	MgF_2
L3	40	100	MgF_2
L4	40	100	MgF_2

NOTE.- These are commercial coated lenses from Edmund Optics made of materials N-SF5 and N-BK-7.

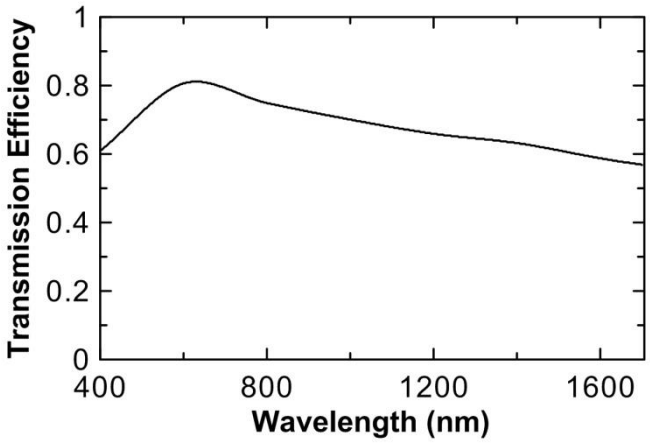

FIG. 5.- Transmission efficiency of the collimating system.

2.2.2 Dichroic element

A dichroic element manufactured by Omega Optics Inc is used, with a nominal cut-on at 950 nm, a reflection ≥ 95% from 400 – 890 nm and maximum transmission between 1000 – 2000 nm for an angle of incidence (AOI) = 45°. The circular dichroic has a diameter of 50.0 mm and a clear aperture of 47.0 mm. Other relevant parameters are its thickness (6.0 mm) and flatness (1/8 wave at 633 nm before coating). Figure 6 shows the transmission curve for the dichroic.

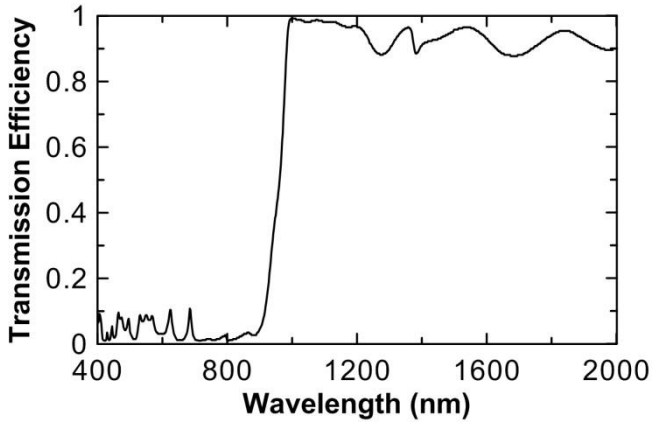

FIG. 6.- Dichroic spectral transmittance curve.

3. VISIBLE CHANNEL IN PLANETCAM 1 AND 2

Considering that the observation of bright objects like planets is the main objective of *PlanetCam*, the detector selected for the visible channel is a scientific CMOS (sCMOS). Compared with CMOS, CCD or EMCCD detectors, the sCMOS is able to use bigger arrays with greater dynamical range providing an excellent combination of fast acquisitions over a large array. A Neo sCMOS detector from ANDOR is used, with a high frame rate, large size, good spectral quantum efficiency and low-noise (1.5 e/s). The detector is an array made of 2,560 x 2,160 pixels (6.5 μm size each) able to provide up

to 100 fps (frames per second) in full frame mode. The detector also allows defining Regions of Interest and binning up to 8x8 pixels for weak sources. For bright objects, this detector allows the accumulation of thousands of low noise high quality frames for lucky imaging. However, it must be noted that not much effort has been done in assuring the use of sCMOS technology in the astronomical context (Qiu et al., 2012). In particular, the linearity in the response of the detector with different exposure times and electronic gains needs to be calibrated. Considering the fast evolution of the detectors technology available, *PlanetCam* has been designed in such a way that allows an easy substitution if required in the future.

3.1 sCMOS radiometric characterization

A laboratory analysis has been performed at the Photonics Laboratory in the Faculty of Engineering at the University of the Basque Country in order to precisely characterize the response of the *PlanetCam* main components, namely, the sCMOS detector, the filters and lenses. Since there is a lack of information with respect to the sCMOS behavior under astronomical circumstances and sensitivity curves provided by the manufacturer do not include data below 400 nm, this was a major step to fully characterize *PlanetCam* visible channel. The spectral response of the sCMOS detector was obtained by capturing, at a fixed exposure time, the radiation provided by a monochromator while scanning the visible wavelength range. The sCMOS relative sensitivity curve was obtained in laboratory (Figure 7), while the maximum Quantum Efficiency value at 550 nm was assumed to be 0.57 according to the manufacturer. At the ultraviolet atmospheric cutoff at ~ 380 nm the detector has QE ~ 0.10.

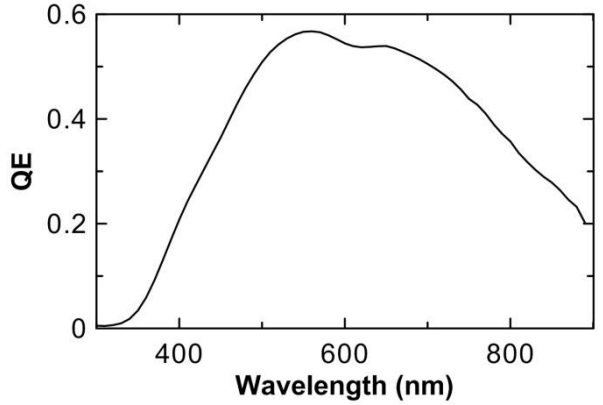

FIG. 7.- sCMOS Quantum Efficiency (QE) as measured in the laboratory.

The sCMOS detector has different electronic gain combinations (ANDOR, 2012). A linearity test has been performed for the sCMOS detector for the minimum electronic gain configuration. The maximum pixel count rate has been registered for different exposure times and incident wavelengths, constraining the range where the sCMOS has a linear response (Figure 8). Because of the variety in the brightness of planetary targets (that depend also on the filters used, see following sections), the camera gain mode can be modified according to the observation circumstances. Therefore the linear response performances of the detector vary accordingly. In most cases the linear behavior occurs at 85% of the maximum counts for different combinations of electronic gains. A full discussion of the camera linearity will be presented elsewhere in a study dedicated to planetary photometry.

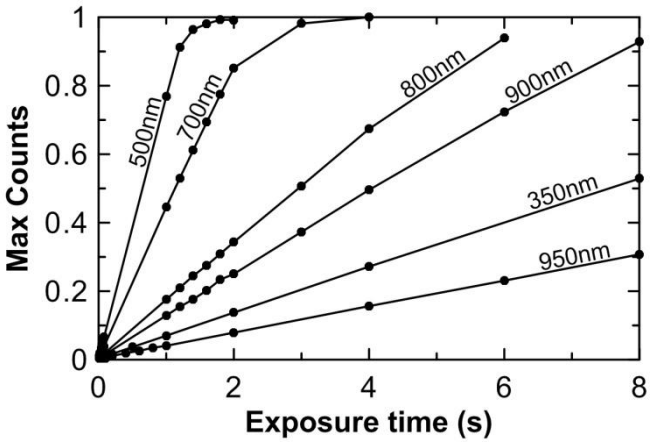

FIG. 8.- The sCMOS count rate measurements as a function of the exposure time at selected wavelengths using a monochromator at the laboratory. The curves have been traced to show the linear range of the detector.

3.2 Visible channel filters

PlanetCam1 works with two filter wheels with 8 positions each, whereas *PlanetCam2* visible channel uses a single larger filter wheel with 20 positions. The filters (1.25 inches in diameter) have been selected according to the interest of particular wavelengths to study planetary atmospheres. Broad-band filters allow high photon transmission making a "lucky imaging" filter series that can be used to fully exploit this methodology and attain high-resolution observations. Additionally, we use narrow band filters centered at wavelengths with some gaseous absorption bands and aerosol

related phenomena, relevant for the observation of planetary atmospheres. Lucky imaging for such situation is restricted to a few filters, low magnifications, the brightest planets, and the use of a large telescope for high rate photon capture. Figure 9 and Table 2 show the filters spectral transmittance and main parameters.

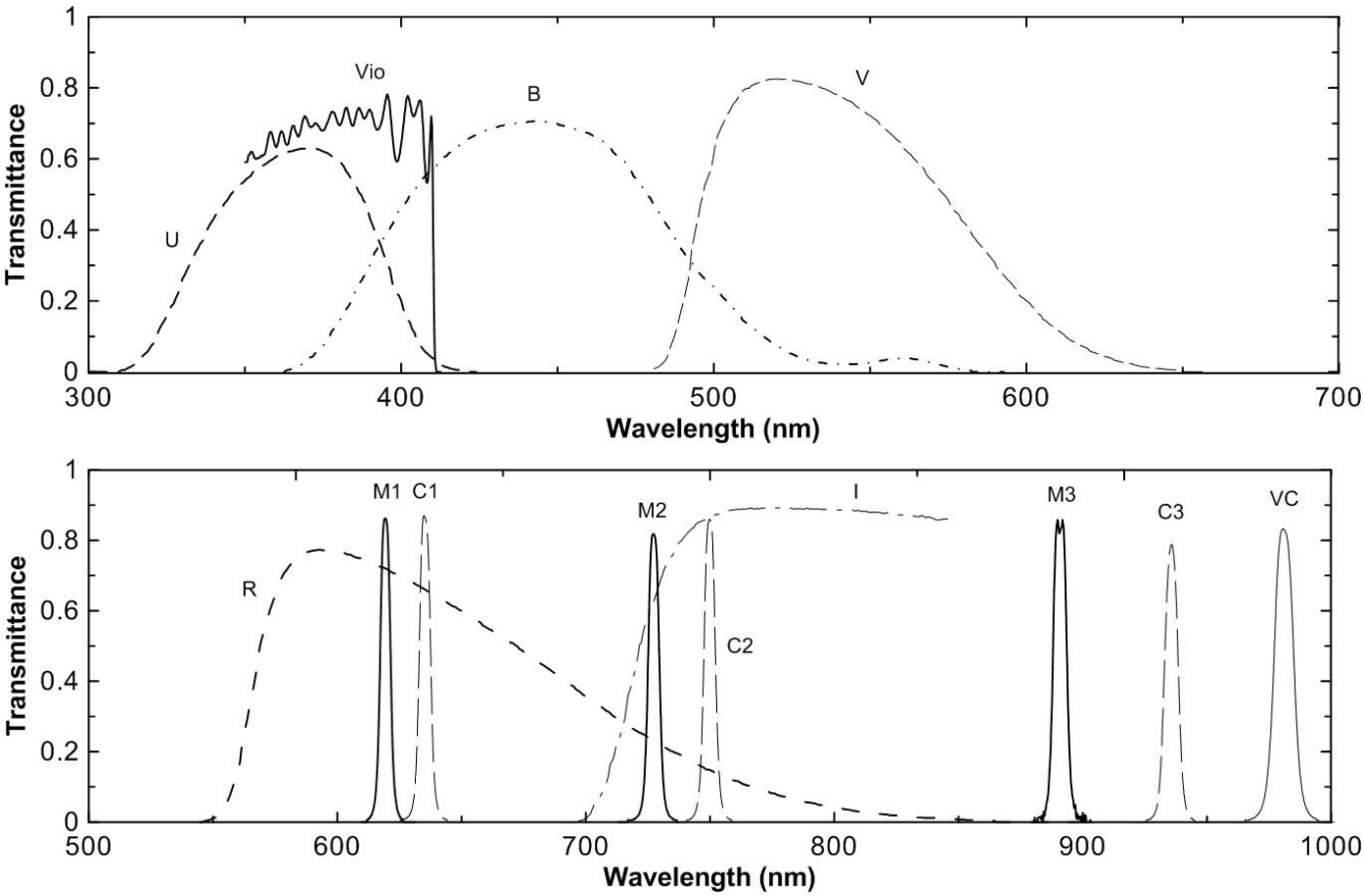

FIG. 9.- Spectral transmittance of the filters used in the visible channel (manufactured by Omega Optical Inc., USA).

The filters of the 'Lucky Imaging' series are common astronomical filters usable for other purposes. For example the B, V, R and I Bessel filters set is usually employed to make color composite images of the planets, as well as standard stellar photometry. When coupled to the detector response curve, they provide in general good contrast and high photon rate on planets that guarantees the use of the lucky imaging technique (Mousis et al., 2014).

There are three filters in the "lucky imaging" series in Table 2 that deserve particular comments (U, Vio and IH-long bandpass from 850nm). The Vio filter covers the spectral range below 410 nm down to the atmospheric and detector cut-off, complementing the classical U (ultraviolet) and B (blue) bands, placed at both wavelength sides. Those wavelengths are extremely interesting to capture images where chromophore agents strongly absorb solar radiation as in Jupiter and Saturn (Simon-Miller et al. 2001a, 2001b; Strycker et al., 2011; Ordoñez et al., 2015) and Venus (Travis, 1978; Titov et al, 2012). The Vio filter also provides high contrast for detection of cloud features on Mars (Parker et al., 1999; Sanchez-Lavega et al., 2015). The U-Vio-B absorption range allows to characterize a particular type of absorbing aerosols of unknown origin in the giant planets and Venus whose spatial distribution seems to be related to particular dynamical features (García-Melendo et al., 2009; Hueso et al. 2009; Pérez-Hoyos et al., 2009; Sánchez-Lavega et al., 2013). Ultraviolet markings on Jupiter and Saturn serve as tracers of high hazes motions at higher altitudes than those tracked with clouds seen at green-red wavelengths (Barrado-Izagirre et al., 2013; Garcia-Melendo et al, 2013; Peralta et al., 2007; Sánchez-Lavega et al., 2008, 2013). However the QE of the camera in the U filter is too low and images require long exposure times of several seconds per frame even at the 2.2 m telescope at Calar Alto. Finally, the IH filter is intended for the observation of the icy giants Uranus and Neptune, since it integrates the continuum with the methane absorption bands located in the red side of the spectrum favoring the observation of atmospheric features that are otherwise difficult to see when using 1-m to 2-m

class telescopes (Sromovsky et al., 2012; Mousis et al., 2014).

Table 2

PLANETCAM2 VISIBLE CHANNEL FILTERS

Filter	$\lambda_{central}$ (nm)	FWHM (nm)	Description
Lucky Imaging:			
U	380	40	Ultraviolet
Vio	400	20	Violet observations
B	445	94	Standard Photometry
V	551	88	Standard Photometry
R	658	138	Standard Photometry
I	-	-	Standard Photometry
IH	-	-	Standard Photometry
Narrow Band:			
M1	619	5	Methane band
C1	635	5	Methane continuum
M2	727	5	Methane band
C2	750	5	Methane continuum
M3	890	5	Methane band
C3	935	5	Methane continuum
VC	980	10	Venus

With respect to the 'Narrow band' series, most of the selected filters are designed to isolate methane absorption bands in the giant planets and Titan with increasing depths at the 619, 727 and 889 nm (M1, M2, M3), coupled to their adjacent continuums (C1, C2, C3), mostly free as much as possible of the methane absorption (Karkoschka, 2010). These filters are used for the observation of the giant planets Jupiter (West et al., 1980) and Saturn (West 1982, 1983; West et al., 1983). Observations in these wavelengths peel-off the atmosphere sensing levels from the lower stratosphere to the upper troposphere (Pérez-Hoyos et al., 2005; Sanz-Requena et al. 2012) where many interesting meteorological phenomena are strikingly visible (e.g. Sánchez-Lavega et al. 2008, 2011; Pérez-Hoyos et al., 2012).

The combination of filters from both series allows high-resolution observations of atmospheric dynamics and vertical cloud structure at mid-resolution. For the giant planets, photometry in the U, B, M3 and R or I filters can be used to calculate color and altitudes indexes for atmospheric features in the giant planets (Sánchez-Lavega et al., 2013). For Venus, the Vio (also complemented by the U filter) and VC (980nm) filters provide high resolution images for cloud dynamics at two vertical levels giving vertical wind shear measurements (Belton et al., 1991; Sánchez-Lavega et al., 2008; Hueso et al., 2012, 2014). Additional filters with a 1.25-inch diameter can be mounted providing a good versatility to the instrument.

3.3 Magnification Optical Systems

In order to achieve the maximum angular resolution, the plate scale provided by the telescope focal ratio should match the detector pixel size in order to get an adequate image sampling. For planetary imaging, sampling is usually close to the Nyquist criterion, i.e. sampling frequency is greater than twice the maximum frequency of the input signal, which in this case means that the diffraction limit should be covered by at least two pixels. Therefore, the recommended focal length (mm) of the telescope is given by $f(\lambda)=2000\ L_{px}D/\lambda$, being L_{px} the pixel size (μm), D the telescope objective diameter (mm) and λ the wavelength (nm). Our sCMOS detector has L_{px} = 6.5 μm, and this recipe gives a focal length of ~ 26 m for a 1 m-diameter telescope working at a wavelength of 500 nm. Since the telescopes where *PlanetCam* is expected to work range from f/8 (1,23m and 2.2 m telescopes at Calar Alto Obs.) to f/17 (1m at Pic du Midi Obs.), magnification optical systems are required to extend the effective focal length. It must be noted however, that this discussion assumes that lucky imaging is able to overcome the limitations of seeing during the observations. This is not very likely to be the case for large-aperture telescopes and an improvement factor of 4 to 5 with respect to seeing is a more realistic situation (Hormuth, 2007). All in all, a range of effective focal lengths from 10 m to 30 m is

desirable in order to accommodate not only the telescope focus but also the local conditions at the observation time.

3.3.1 Magnification in PlanetCam1 visible channel

The solution designed for this case was to have a number of manually interchangeable Barlow lenses (divergent optical combinations) with magnifications from 2 to 4. The maximum amplification is provided by a commercial *Baader Planetarium Fluorite Flatfield Converter Barlow* (BPFFC), which is formed by two doublet lenses providing a magnification of 4 and a diffraction-limited, apochromatic flat field over a 90 mm image circle. For lower amplifications we use commercial *Thorlab lenses* ACN254-050-B with a 50 mm focal length providing similar amplification to BPFFC, as well as ACN254-075-B (75 mm focal length) and ACN254-100-B (100mm focal length). All these lenses are negative achromatic doublets, and the anti-reflection (AR) coating is optimized for the near infrared side of the visible channel (650-1050 nm).

3.3.2 Magnification in PlanetCam 2 visible channel

The solution adopted for *PlanetCam2* optical magnification is different. It consists of three interchangeable optical elements (convergent ocular projection systems) whose position is motorized and electronically controlled by software. The lens system is selected by means of a lateral displacement motor (elements 2, 3, 4 and 9 in Figure 3). Essentially *PlanetCam2* visible channel provides three magnifications ranging from 1.18 to 2.65.

When used at the Calar Alto Observatory 1.23 m and 2.2 m diameter telescopes, they provide a plate scale ranging from 4.4 to 17.7 arcsec/mm and field of views (FOV) from 72 to 144 arcsec without vignetting. This guarantees that all the planets can be fully imaged. At maximum amplification, the scale at the plane detector is 0.028 arcsec/pixel well below the diffraction limit of the 2.2m telescope.

4. THE SHORT-WAVE INFRARED CHANNEL (SWIR) IN PLANETCAM 2

The beam direction for the Short Wave Infrared (SWIR) channel is at 90° with respect to the visible channel one so, after the beam split by the dichroic, it passes through the filter wheel and the magnification optical system before entering the SWIR detector (Figures 2 and 3). The individual elements of the SWIR channel are described in the following sections.

4.1 SWIR detector

For the SWIR channel detector we selected the commercial camera OWL SWIR 640 manufactured by Raptor Photonics. The detector is an InGaAs PIN-photodiode with an area size of 640x512 pixel square elements (9.60 mm x 7.68 mm), of 15 x 15 μm each. The spectral range coverage extends from 0.4 μm to 1.7 μm with peak QE ~ 85% at 1.35 μm (Figure 10). The digital output format is 14 bit with a readout noise < 50 electrons (high gain mode). The faster frame rate is 120 Hz and exposure times range 8.5 ms – 22 s. Longer exposure times are not possible due to detector saturation by the dark current. For astronomical purposes the detector is cooled down at an operational temperature of -15°C using a cooling water circuit and a cool plate. The camera incorporates a gain control and on-board dynamic 3 point Non Uniform Correction (NUC) based on a baseline offset, gain and dark current calibrated for this temperature. Nevertheless, low light images or long exposures require additional dark currents calibration and flat fielding.

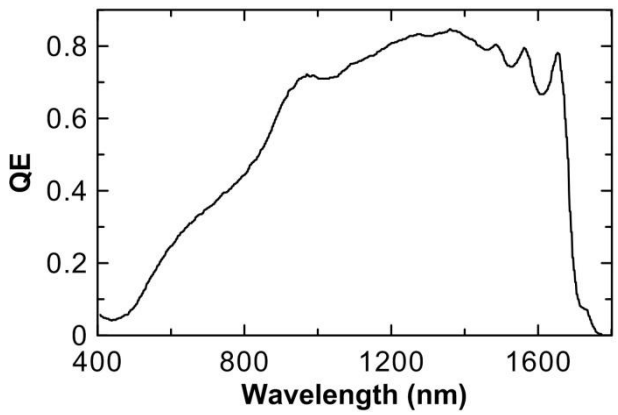

FIG. 10.- Spectral Quantum Efficiency (QE) of the SWIR detector as provided by the manufacturer.

4.2 SWIR Filters

SWIR filters were selected to isolate particular absorption bands in planetary atmospheres (essentially CO_2 for Venus and CH_4 for the giant and icy planets and Titan), and at the same time to work in two complementary modes, lucky imaging for high spatial and temporal resolution (broad-band filters), and short sequences of longer exposures required in deep absorption bands. Table 3 lists the SWIR filters and their main purpose and Figure 11 shows their spectral transmittance curves. Some of the observing bands are also affected by water absorption in Earth's atmosphere and are only available for images under exceptionally dry conditions.

Table 3

PLANETCAM2 SWIR CHANNEL FILTERS

Filter	$\lambda_{central}$ (nm)	FWHM (nm)	Description
Lucky Imaging:			
RG1000			Long red bandpass >1μm
J			Standard photometry
H			Standard photometry
Narrow Band:			
YC	1090	30	Methane continuum (C4) (*)
YM	1160	40	Methane band (M4)
V1	1190	20	CO2 continuum
V2	1220	50	CO2 band
JC	1275	50	Methane continuum (C5)
JM	1375	50	Methane band (M5) (*)
V3	1435	20	CO2 band (*)
HC	1570	50	CO2 continuum
			Methane continuum (C6)
HM	1650		Methane band (M6)
			Long red bandpass >1.62μm detector cut.

* Affected by water absorption in Earth's atmosphere.

The SWIR wavelength range is very well suited for capturing high clouds in the outer planets and Titan, as well as for studying their properties using a combination of methane absorption band filters and their adjacent continuums. A similar procedure can be use in Venus with the CO_2 absorption bands. In addition, the night side of Venus can be imaged with filters in the range 1 – 1.2 μm to capture surface features (Helbert et al., 2008) and at 1.27 μm to map the atmospheric airglow emission (Gerard et al., 2008; Hueso et al., 2008).

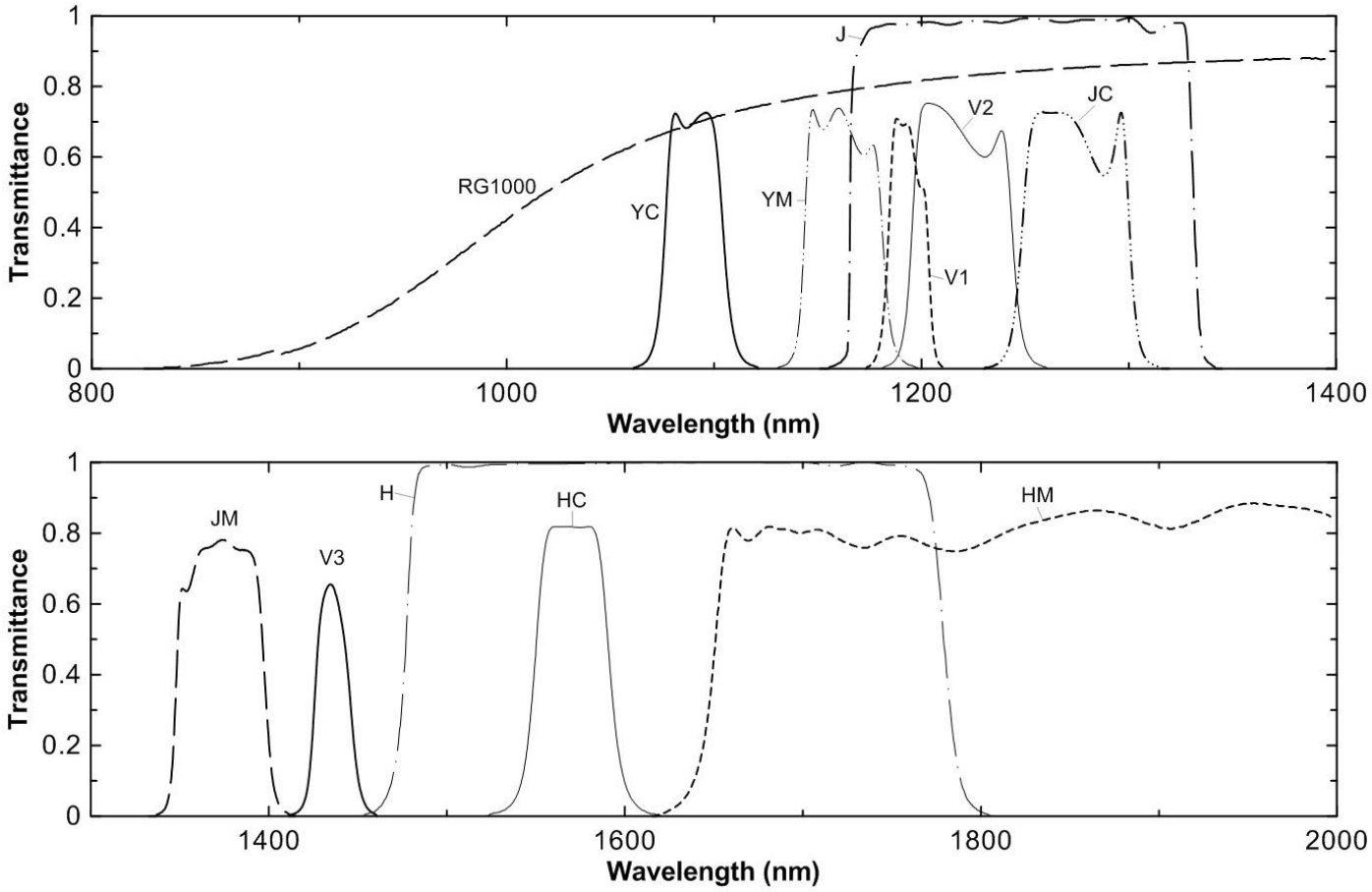

FIG. 11.- Spectral transmittance of the filters used in the SWIR channel.

4.3 Magnification in PlanetCam2 SWIR channel

Similarly to the visible channel, the SWIR channel on *PlanetCam2* has three interchangeable magnifications made by convergent projection systems whose position is motorized and electronically controlled by software independently from the visible channel. The lens system is selected by means of a lateral displacement (elements 5, 6, 7 and 11 in Figure 3). Essentially, *PlanetCam2* SWIR channel provides three magnification possibilities ranging from 1.10x to 2.00x. When used at the Calar Alto Observatory 1.23 m and 2.2 m diameter telescopes they provide a plate scale ranging from 5.86 to 19.0 arcsec/mm and field of views (FOV) from 56 to 144 arcsec, as for the visible channel. This guarantees that all the planetary disks can be imaged in a single exposure. The comments made for the VIS field of view vignetting are also applicable here. At maximum amplification, taking into account that the OWL Raptor camera has a pixel size of 15 μm, the scale at the plane detector is 0.088 arcsec/pixel.

5. CAMERA CONTROL

PlanetCam1 is controlled by means of a GUI based on LabView which provides full control for the detector and the filter wheel. This GUI allows the user to acquire sequences of images and to program series of acquisitions in different filters. The interface also allows defining binning and regions of interest over the image as well as zoom over the actual image that it is being acquired. It is also possible to control the temperature of the Andor detector, and to turn on/off the fans. The code is based on the software development kit provided by the manufacturer while the filter wheel control software was designed from scratch.

The mechanic devices that constitute *PlanetCam2* are controlled by a simple electronics module located at one side of the instrument (Figure 2). The visible and SWIR modules are identical to each other and are controlled by two PCs. The main component of each module is the motor controller of the focus and optical selector stages, and is based on an ARDUINO microcontroller and a stepper shield. In order to minimize the external connectors, a USB hub is included to collect the signals from the filter

wheel and the ARDUINO board. Cameras connection with the PCs is done using CameraLink communications protocol ensuring a fast data transfer. The PC controlling the visible detector has solid state disks to maximize the speed of data storage. Each detector is controlled through custom design software written in C++ which allows the instruments to acquire simultaneous sequences for both channels and control the mechanics and optics of the instrument. The graphical interfaces are identical for the Visible and SWIR channels, and the detectors control is based on the software development kits from their respective manufacturers. This software allows the following functionalities:

- Selection of optical resolution: The software moves the focus and the optical selector stages for each arm to the proper positions for each configuration.
- Display and control of the internal temperature values of the detectors.
- Selection of filter.
- Display of the acquired frames: Visualization is done at a maximum rate of 0.5 Hz for the visible channel and the acquisition rate for the SWIR channel.
- Acquisition of sequences of images with a given exposure time, gain, number of frames, as well as selection of region of interest and binning in the visible channel.
- Zoom over cursor position.
- Data saving in standard FITS cubes (Flexible Image Transport System).

6. LUCKY IMAGING PROCESSING

Images are processed with a pipeline written in IDL (Interactive Data Language) specifically designed for *PlanetCam* but also suitable for analysis of data from other lucky imaging cameras such as AstraLux (Hormuth, 2007). The software is called PLAYLIST (PLAnetarY Lucky Images STacker) and is used to analyze without human interaction the large sequence of observations obtained in a given observing night. PLAYLIST builds a list of files from a selected folder, but it can also be used to analyze a single file. For each file, PLAYLIST finds the proper dark current and flat files to be used in the image reduction. Each frame is reduced with the corresponding dark and flat. Hot and cold pixels that could remain after the frame reduction process are identified and removed with an adaptive median filter technique. Frame quality is analyzed using a metric based on the Sobel filter (González and Woods, 2008), which is a first estimation of the brightness gradient of an image and is a fast measurement of image sharpness.

The software allows Lucy Richardson deconvolution (Richardson, 1972; Lucy, 1974) on a frame by frame basis but this option is generally not used since it requires bright images with low levels of noise. The planet or object of interest is automatically located with an algorithm based on the evaluation of the center of brightness of the image which is precise to a few pixels. Images are co-registered using an image correlation algorithm that is applied to the central part of the planet or object. PLAYLIST also allows correlation of images based on several points by moving each frame into a reference image initially created from a subset of the images. This procedure corrects image distortions created by the atmospheric seeing in large objects like Jupiter. For each image sequence PLAYLIST generates several FITS files with different levels of image quality by selecting only the best 1%, 2%, 10%, 30% or all frames in the sequence. A full night of observations with the SWIR channel can be analyzed with a standard computer in a few hours. Observations with the VIS channel at large spatial resolution are more demanding requiring a few days for a typical observing campaign. The software can also be used to produce a quick analysis of images at the telescope, while acquiring the observations. This is useful to judge exposition time values used and observation strategies depending on the object and atmospheric seeing. The quick analysis does not perform dark or flats corrections, deconvolution or image warping and simply stacks the images using the center of brightness algorithm for coregistration of the frames. PLAYLIST will be publicly released and described extensively elsewhere (Hueso et al. in preparation).

7. ASTRONOMICAL CHARACTERIZATION OF PLANETCAM

In this section the first astronomical tests performed are described, with the camera in its different available modes in order to characterize its performance with real targets.

7.1 PSF and resolution on stars

The combination of the object being observed, the diffraction pattern of the telescope and the atmospheric seeing produces a light intensity distribution map in the detector plane. For point sources, the pattern is described by a Point Spread Function (PSF) which, under normal conditions, has radial symmetry and can be represented by a weighted sum of a Gaussian function and a Moffat profile (Hormuth 2007, 2008). For lucky imaging applications, Law et al. (2006) showed that the PSF of a star improves with a selection of frames based on their quality (lower Gaussian FWHM).

The resolution of the camera has been tested with the double star STF439 (HD281159, magnitude V = 8.80 and 10.30, separated 0.6", WDS2014) with *PlanetCam2* –Visible channel at CAHA 2.2 m telescope and normal seeing conditions. In total 1000 frames were taken with 0.1s frame exposure time. Figure 12 shows the PSF fitting to both stars for different image quality thresholds measured by the percentages of selected images according to their quality. Seeing limited and diffraction limited profiles are also shown for comparison. Using the best frames the PSF fitting improves, reducing FWHM from 0.51 arcsec to 0.39 arcsec (using 100% frames to the best 1%), and increasing Strehl ratios from 7.1% to 11.7% for star STF439A (100% frames stacked to the best 1%), and from 5.8% to 9.1% for STF439B. Although the resolution improvement by comparison of Strehl ratios is only modest (2.2 in this example) the quality of the images is undoubtedly much better in the lucky imaging result.

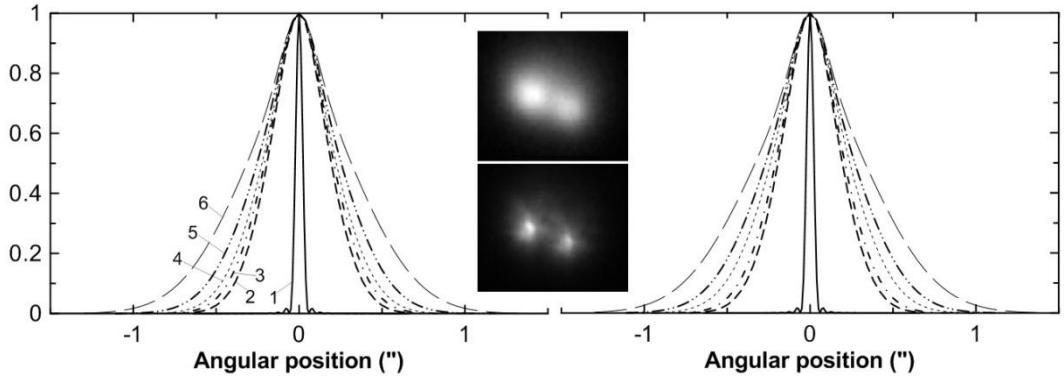

FIG. 12.- The normalized PSF profiles for the double star STF439 (left A, right B) at CAHA2.2m (Dec. 2014) with PlanetCam2 for different percentage frame selection levels and the seeing limited images. Seeing limited images formed by adding all images in the sequence without computing their relative shifts, and PSF profiles for the diffraction limit are also shown: 1- Diffraction limited, 2- Best 1%, 3- Best 10%, 4- Best 30%, 5- All stacked, 6- Seeing limited. The double star picture in the centre shows the result of the seeing limited image (up) and that from best 1% frame selection (down).

7.2 Resolution on planetary images

Planets are extended objects so resolving details on planetary images depends not only on the resolving power of the instrument, as ideally dictated by diffraction (through Rayleigh criterion valid for two sources of equal brightness), but on the intensity contrast between a given feature and its background. The spatial resolution and contrast performance of an optical system are described by the Modulation Transfer Function (MTF) represented as a function of the spatial frequency (Smith, 2000; see D. Peach description in reference to Solar system observations http://www.damianpeach.com/simulation.htm, 2015). We have tested the capability of *PlanetCam2* to resolve atmospheric features on our best images of Jupiter, which is so far the most observed target with our instrument. With the 2.2m telescope, under good seeing conditions we typically resolve in the visible range contrasted features with a size ~ 0.25 – 0.30" (about 800 km in Jupiter) (see details in section 8, Figs. 18 and 22). At this resolution, *PlanetCam2* allows to study the cloud structure, dynamics and meteorological phenomena at the synoptic scale on most planetary atmospheres.

7.3 Astrometry

The uniformity or flatness of the field of view (FOV) given by the camera has been tested performing astrometry on a known calibrated star field. This analysis has been performed for the visible sCMOS detector in both configurations

PlanetCam1 and *PlanetCam2* on the open cluster M103. Figure 13 shows the central field of the cluster M103 imaged by both configurations. The stars are identified by capital letters and the measured angular distance between selected pairs has been identified using the International Celestial Reference System (Souchay and Feissel-Vernier, 2006).

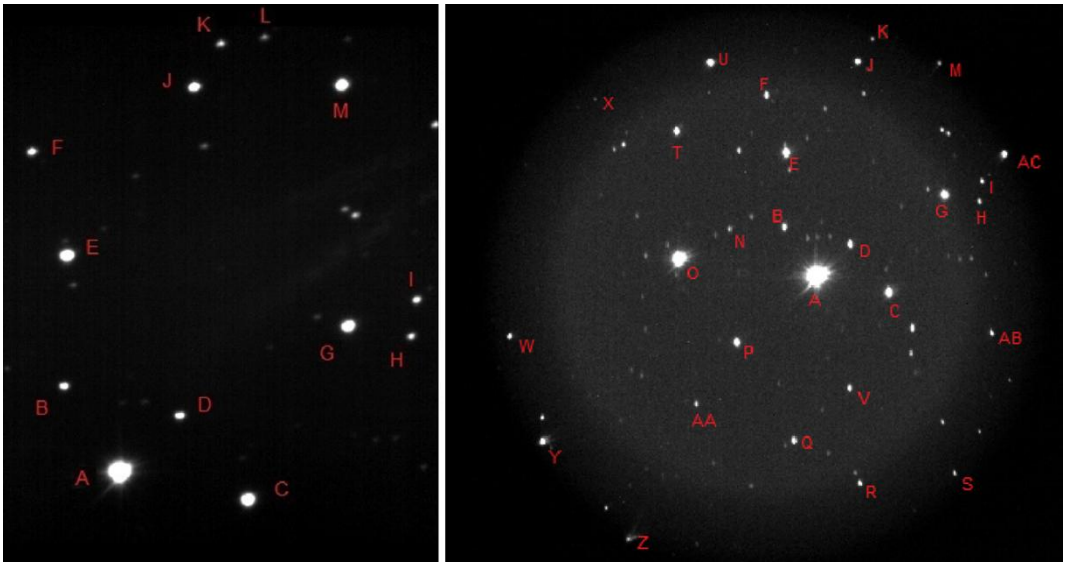

FIG. 13.- M103 cluster in images taken at CAHA 1.23 m telescope at visible wavelengths (sCMOS detector). Left with *PlanetCam1* and a magnification of 2.7x; Right with *PlanetCam2* at low resolution.

From this analysis a scale of 0.049 ± 0.002 "/pixel was estimated for *PlanetCam1* with 2.7 magnification used, and 0.116 ± 0.007 "/pixel for *PlanetCam2* visible channel in the low resolution mode, both in agreement with the theoretical estimation predicted by this specific optical configuration.

In the non vigneting region, the scale or distance between pairs of stars shows no dependence with the position/orientation of the stars in the image or with the angular separation between the two stars when this value is large enough to neglect the uncertainty in the stars position given by their FWHM. The FOV shows no optical distortion within our detection limits, which is in agreement with the planetary images and their measurements (see section 8).

7.4. Limiting magnitudes

Several tests have been performed on the 1.23 m and 2.2 m telescopes in order to estimate the limiting magnitude for objects potentially to be observed with *PlanetCam* for different optical configurations, filters and exposure times. In Figure 14 we show four examples of the detection of faint objects with *PlanetCam* under different configurations mounted at these telescopes. In the SWIR channel of *PlanetCam2* at the 2.2 m telescope magnitude J ~ 17 can be achieved at maximum resolution (scale 0.088 arcsec/pixel) in 25 s. In the visible channel, magnitude ~ 19 can be achieved in this telescope for exposure time values of few seconds at maximum resolution.

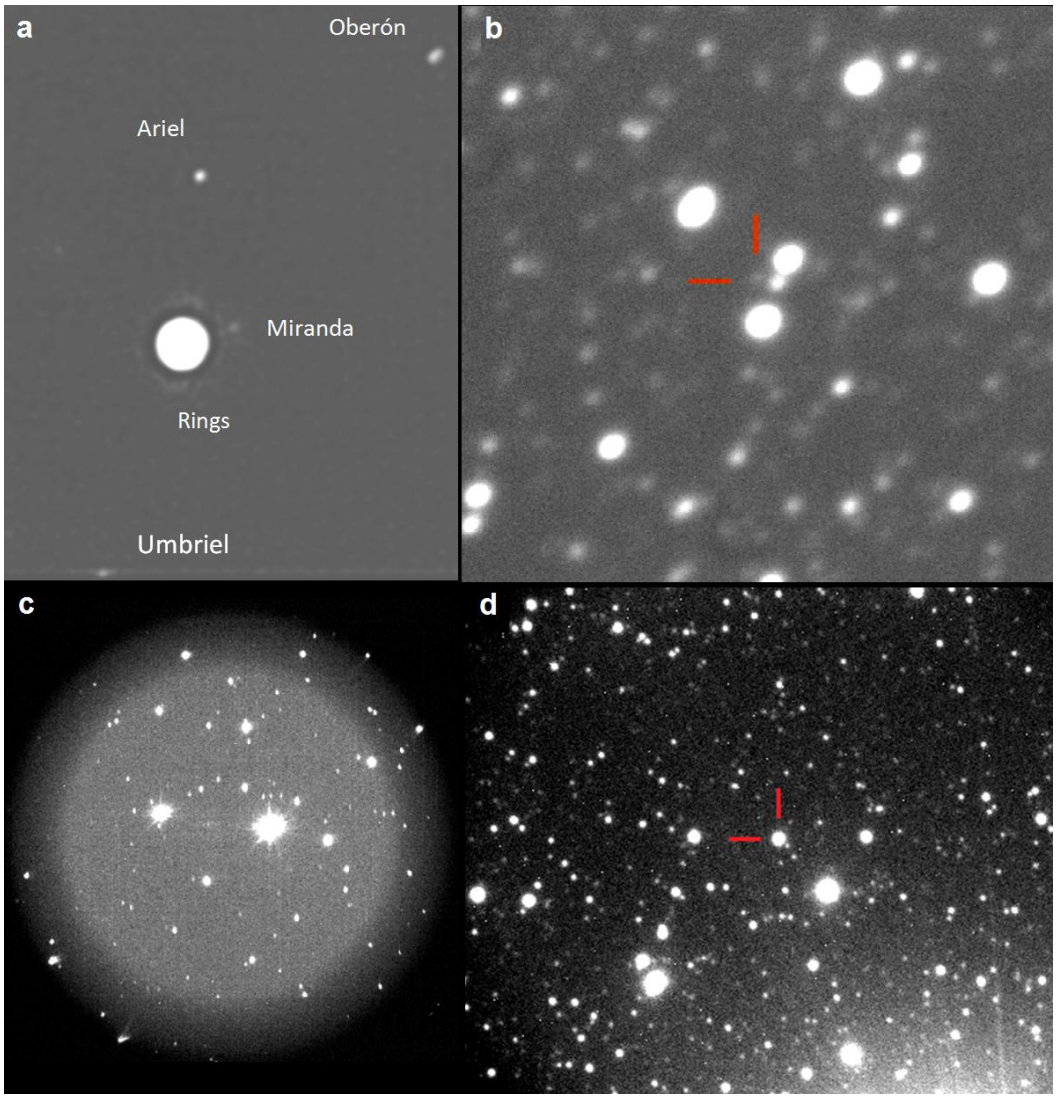

FIG. 14.- Limiting magnitude tests: (1) Uranus and its rings and main satellites including Miranda (magnitude 15.9) observed with *PlanetCam2* SWIR channel and RG1000 filter (2.2 m telescope; 300 exposures of 1 s); (2) Quaoar KBO (magnitude 18.8) with *PlanetCam1* without filter (single frame of 5 s and binning 8x8 during capture; this observing mode has utilities in star occultations observations); (3) Globular cluster M103 in an image taken at CAHA 1.23 m with *PlanetCam2* visible channel at low resolution (180 s from 6 frames of 30s exposure). Stars of magnitude up to 19 can be recognized; (4) Pluto with *PlanetCam1* with no magnification and I-filter at CAHA 2.2 m (single exposure of 512 s). Stars of magnitude over 15 are easily recognized and fainter sources can be identified.

8. IMAGING OF SOLAR SYSTEM OBJECTS

The main goal of *PlanetCam* is the research and survey of phenomena in solar system bodies, in particular the study of the changes in the cloud structure and dynamics of planetary atmospheres. Imaging of the planets at different wavelengths allows studying the aerosol and cloud properties, meteorological phenomena, measurement of global winds and assessments of the spatial and temporal scales of evolution. Absolute radiometric calibration using standard stars allows obtaining the spectral and spatial dependence of the reflectivity across the planet atmosphere (from center-to-limb or north-south scans) or those of particular features (see e.g. Sánchez-Lavega, 2011). Modeling of the absolute reflectivity allows retrieving the cloud and aerosol vertical distribution and their optical properties (Hansen and Travis, 1984; see e.g. our previous studies by Pérez-Hoyos et al., 2005, 2009, 2012).

In what follows we show some examples of images of solar system bodies.

8.1 Terrestrial planets: Venus and Mars

We have imaged Venus with the CAHA 1.23 m and 2.2 m telescopes with *PlanetCam1* with the UV, Violet and methane band filters to detect clouds at different altitude levels above surface (Sánchez-Lavega et al., 2008). Figure 15a shows examples of the cloud morphology at the two spectral ranges and altitude levels sampled: upper cloud (65-70 km, U and Vio filters) and base of the upper cloud (60 km, M3 890 nm).

Mars was imaged with *PlanetCam1* at selected wavelengths during the 2014 opposition. The aim was to look for the capabilities of the camera to capture surface details and atmospheric phenomena (dust and clouds). Figure 15b shows image examples where such features are well detected and easily identifiable. Particularly interesting is the performance of the camera in the U and Vio where the clouds become conspicuous.

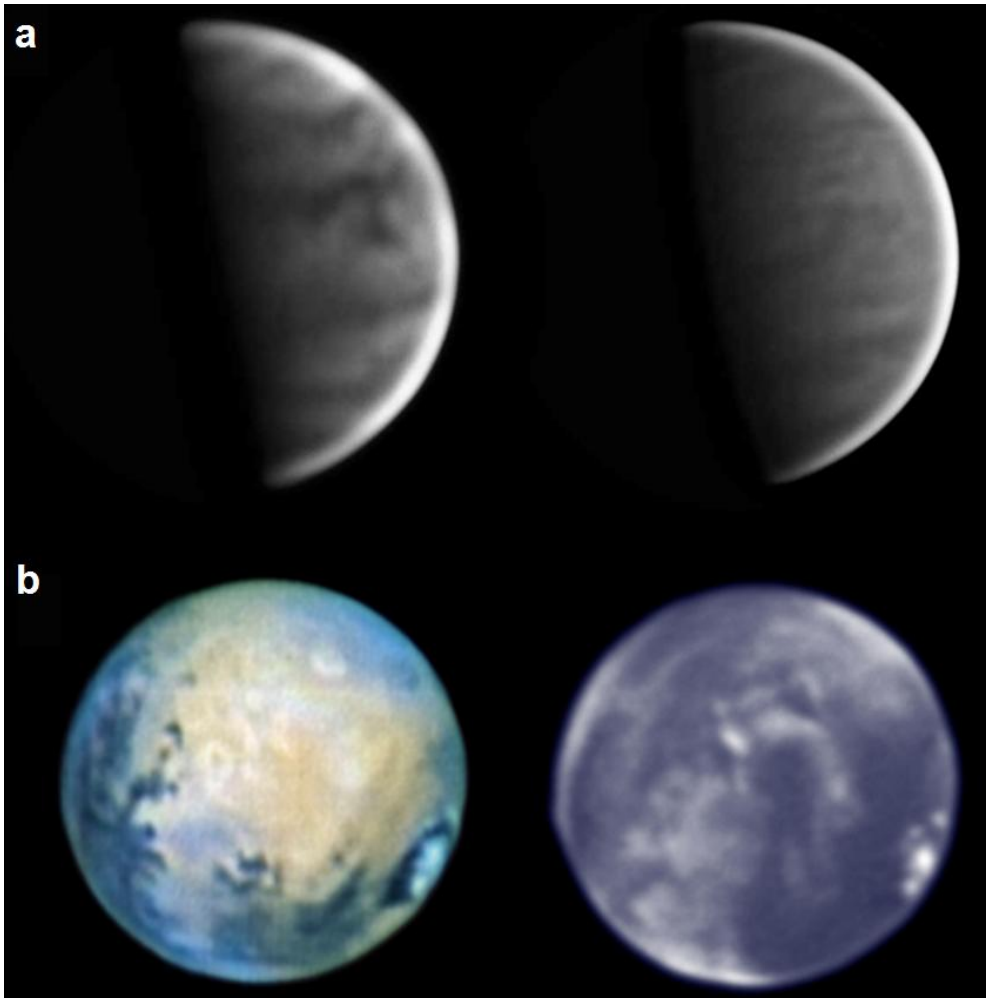

FIG. 15.- (a) Venus on *PlanetCam1* at the 2.2m telescope observed on 2014-04-07. Left panel: U and Vio filters combined into a single image. Right panel: M3 filter (890 nm). Images were acquired at 05:22 UT (left) and 05:33 UT (right). The planet diameter is 20.9" and the observations were acquired with an elevation of 21º and a phase angle of 82º. High-resolution images were built from the best 30% of three acquisitions (U: 300 frames of 0.5 s; Vio: 500 frames of 0.05s; M3: 2000 frames of 0.05s) and were high-pass filtered to show the cloud details. (b) Mars on *PlanetCam1* at the 2.2m telescope observed on 2014-04-07. Left panel: Color composition using Red, Green and Blue filters and a luminosity layer from observations in a red filter acquired at 00:06 UT; Right panel: U observation acquired at 00:39 UT. The planet diameter is 15.0" and the observations were acquired with an elevation of 47º and a phase angle of 82º. High-resolution images were built from the best 30% of the original observations (Wratten21: 1000 frames of 1 ms; U: 200 frames of 2.0s) and were high-pass filtered to show the surface and cloud details.

8.2 Giant and icy planets

The giant and icy planets are primary candidates for *PlanetCam*. High-resolution

imaging in visible and SWIR allows tracking a large number of dynamical phenomena as well as to determine the global motions (wind field structure) at different altitude levels, and study the structure and properties of the cloud cover. Most observing campaigns with *PlanetCam* have focused on Jupiter and Saturn oppositions. Figure 16 shows a typical sequence of Jupiter images to construct a RGB color composite. The figure also illustrates the spatial resolution attained on lucky imaging observations (left panel) and the additional processing that is generally required to extract high-resolution information. Images without processing can be calibrated and used to retrieve the vertical cloud structure. Images processed with a variety of image processing techniques are generally required for dynamic studies. Atmospheric features smaller than 0.4" are resolved. High-contrast small features are resolved easier than low-contrast features of the same size.

Figure 17 shows a series of Jupiter images taken in the same night with filters sensitive to different absorption agents (aerosols and methane gas), Rayleigh scattering, and altitude levels in the atmosphere. These series were photometrically calibrated using standard stars and the procedures and scientific results will be presented elsewhere. Figure 18 shows two high resolution images of Jupiter taken at close wavelengths (890 nm methane absorption, filter M3, band and 950 nm approximately, filter C3) that sense different altitude levels in the atmosphere. The first image series obtained in the SWIR channel of *PlanetCam2* on Jupiter are shown in Figure 19. Some wavelengths are affected by water absorption on Earth's atmosphere, but careful calibration of the narrow band filters between 1090 and 1570 nm that involve methane bands and their adjacent continuum, can be used to retrieve in detail the cloud vertical structure at different latitudes. The filter RG1000 and those at the J and H bands are well suited for high resolution imaging.

Saturn has been imaged at a variety of wavelengths using *PlanetCam1* and *PlanetCam2* (Figure 20). The main goal here is to complement Cassini observations in order to survey for large-scale dynamical phenomena and to study the vertical cloud structure and their long-term changes from photometrically calibrated images. SWIR image of the maximum optical amplification are able to resolve most bands on the planets and details such as the north polar hexagon and polar vortex.

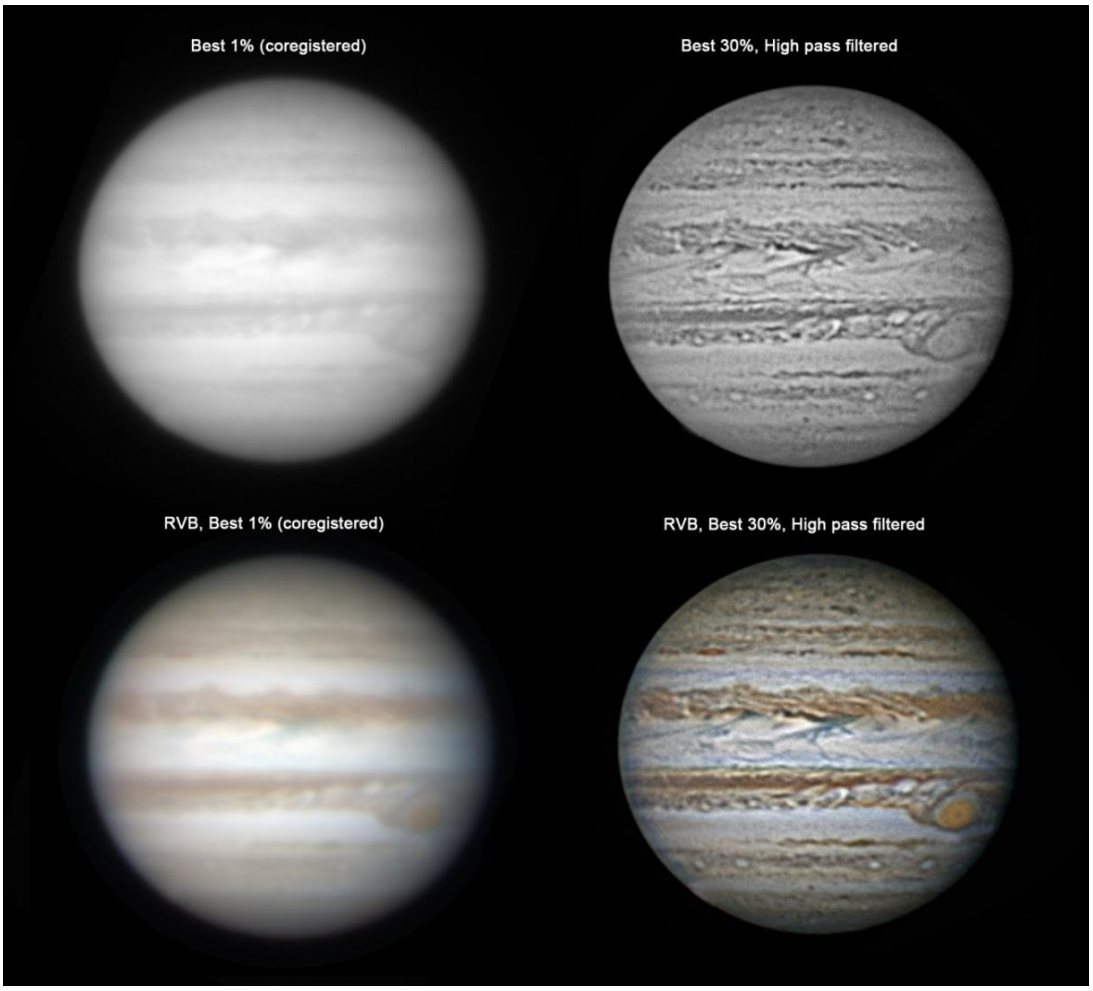

FIG. 16.- Jupiter on *PlanetCam2* at the 2.2m telescope observed on 2014-12-11 at 01:09 UT. Top: Image acquired with a Red filter. Bottom: Color image from R, V, B filters. Top left: Photometric image built from co-registering the best 1% of all frames. Top right: Image built from co-registering the best 30% of all frames and using high-pass filters to increase the visibility of atmospheric cloud features. Bottom left: Photometric color image from the best 1% of all frames. Bottom right: Color composition from the best 30% of R, V, B images using a combination of high-pass filters to enhance the visibility of atmospheric features. The planet diameter is 41.0" and the observations were acquired with an elevation of 40º and a phase angle of 9.6º. North is up and West to the left. Frame exposure times are 0.05 s and typically 500-1500 frames are acquired in sequence.

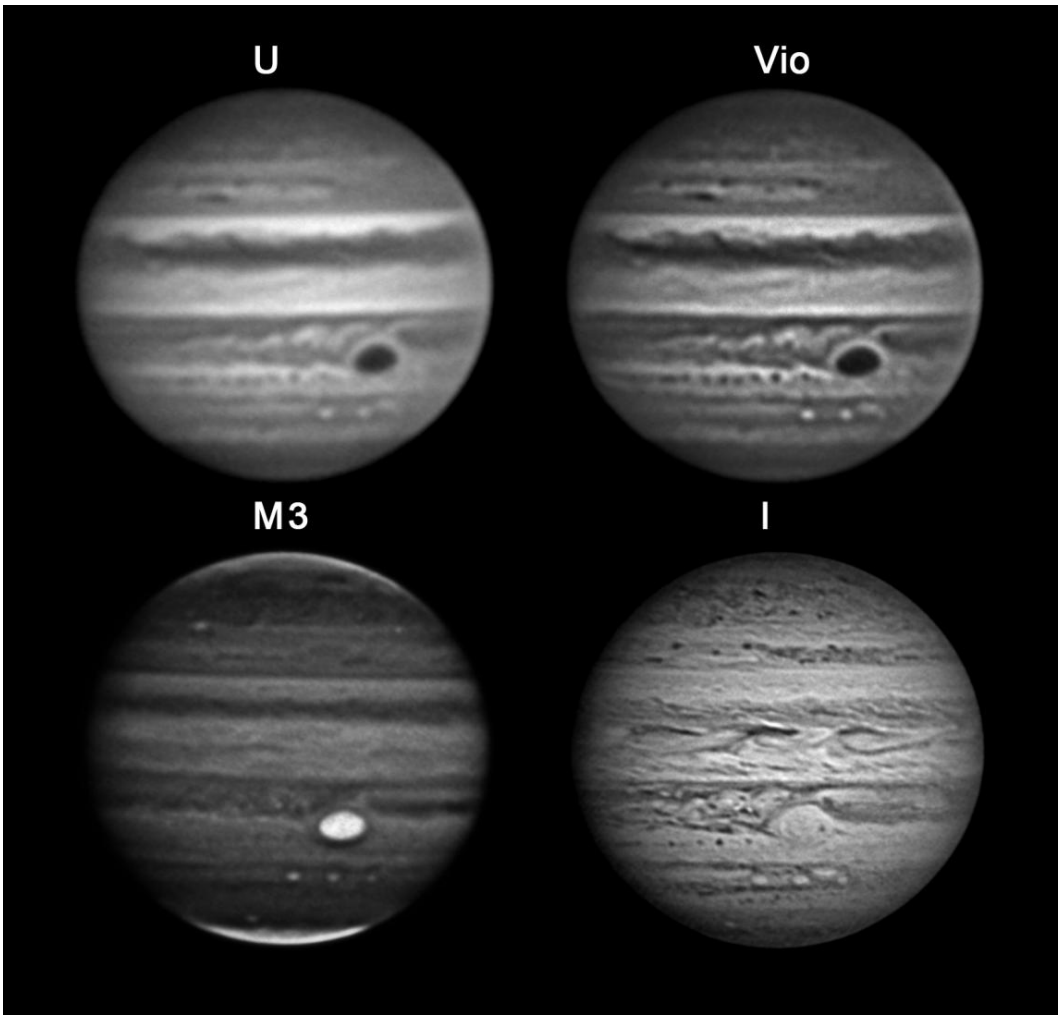

FIG. 17.- Jupiter on *PlanetCam1* at the 2.2m telescope observed on 2014-04-06 at 22:43 UT (UV), 22:11 UT (I) 22:25 UT (M3) 22:39 UT (Vio). All images have been built from co-registering the best 30% of all frames and using high-pass filters to increase the visibility of atmospheric cloud features. The planet diameter is 37.9" and the observations were acquired with an elevation of 32º and a phase angle of 11º. North is up and West to the left. Frame exposure times vary from 0.05 s in the I filter to 5 s in M3.

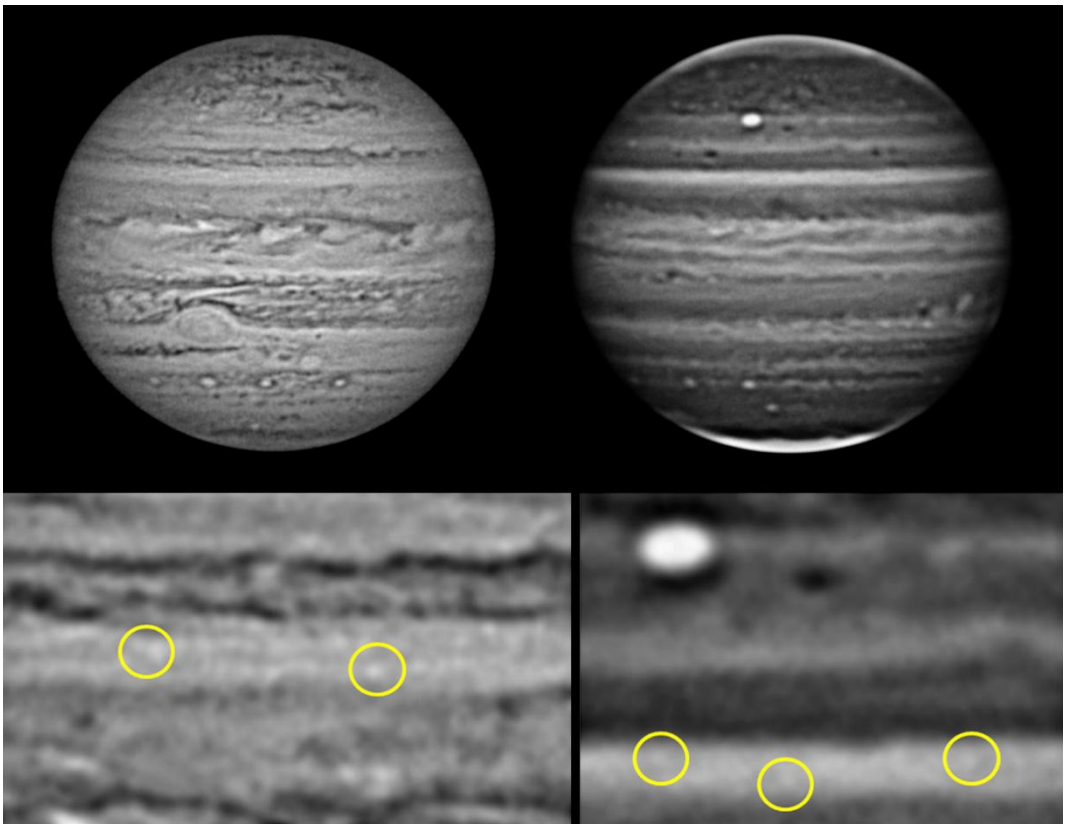

FIG. 18.- Jupiter on *PlanetCam1* at the 2.2m telescope observed on 2012-12-03 on a I filter at 19:53 UT (left) and on a M3 filter at 22:37 UT (right). Images have been built from co-registering the best 30% of all frames and using high-pass filters to increase the visibility of atmospheric cloud features. The planet diameter is 48.5'' and the observations were acquired with an elevation of 36º and 66º respectively and a phase angle of 0.2º. North is up and West to the left. In the lower part a zoomed area of each image is shown with selected (circled) small features having a size of 0.30-0.35 arcsec at the resolution limit of the instrument. Frame exposure times are 0.05 s in the I filter and 10 s in M3.

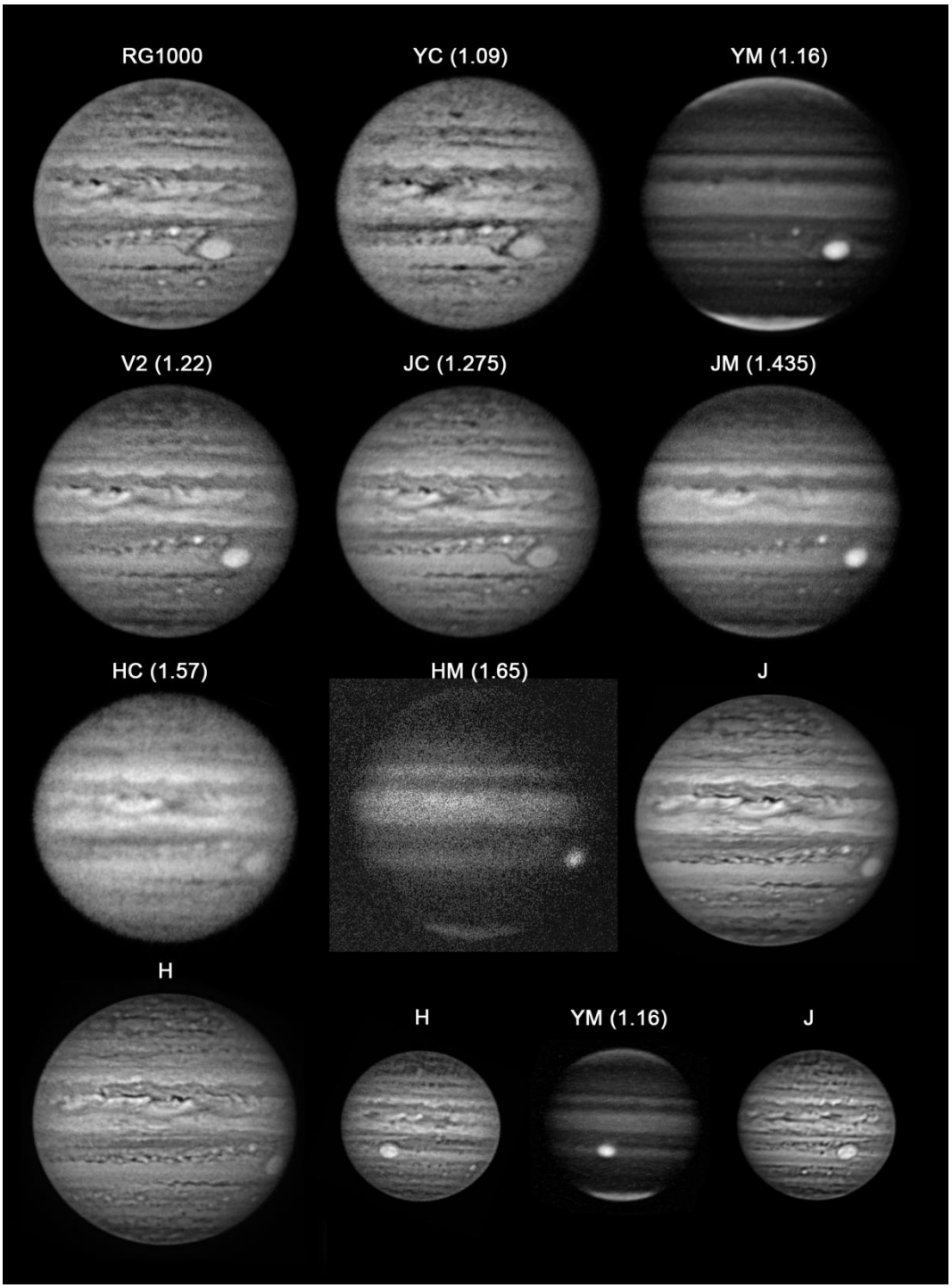

FIG. 19.- Jupiter on *PlanetCam2* at the 2.2m and 1.2m telescopes observed on 2014-12-11 (2.2m telescope, larger images acquired from 00:31 UT to 01:33 UT) and 2015-03-03 (1.2m telescope, smaller images acquired from 20:45 UT to 22:08 UT). Images were built from co-registering the best 1% in bright wide filters (J,H, RG1000) to all frames in dark methane filters (YM) and using high-pass filters to increase the visibility of atmospheric cloud features. In the December 2014 images the planet diameter is 41.0''and the observations were acquired with an elevation of ~50º and a phase angle of 0.7º. In the March 2015 images the planet diameter is 44.4'', its apparent magnitude is -2.50 and the observations were acquired with an elevation of ~65º and a phase angle of 5.0º. Note that the December 2014 images are nearly simultaneous to those on Figure 17. North is up and West to the left. Frame exposure times vary from 8.5 ms in J, H, and RG1000 to several seconds in the YM and HM filters.

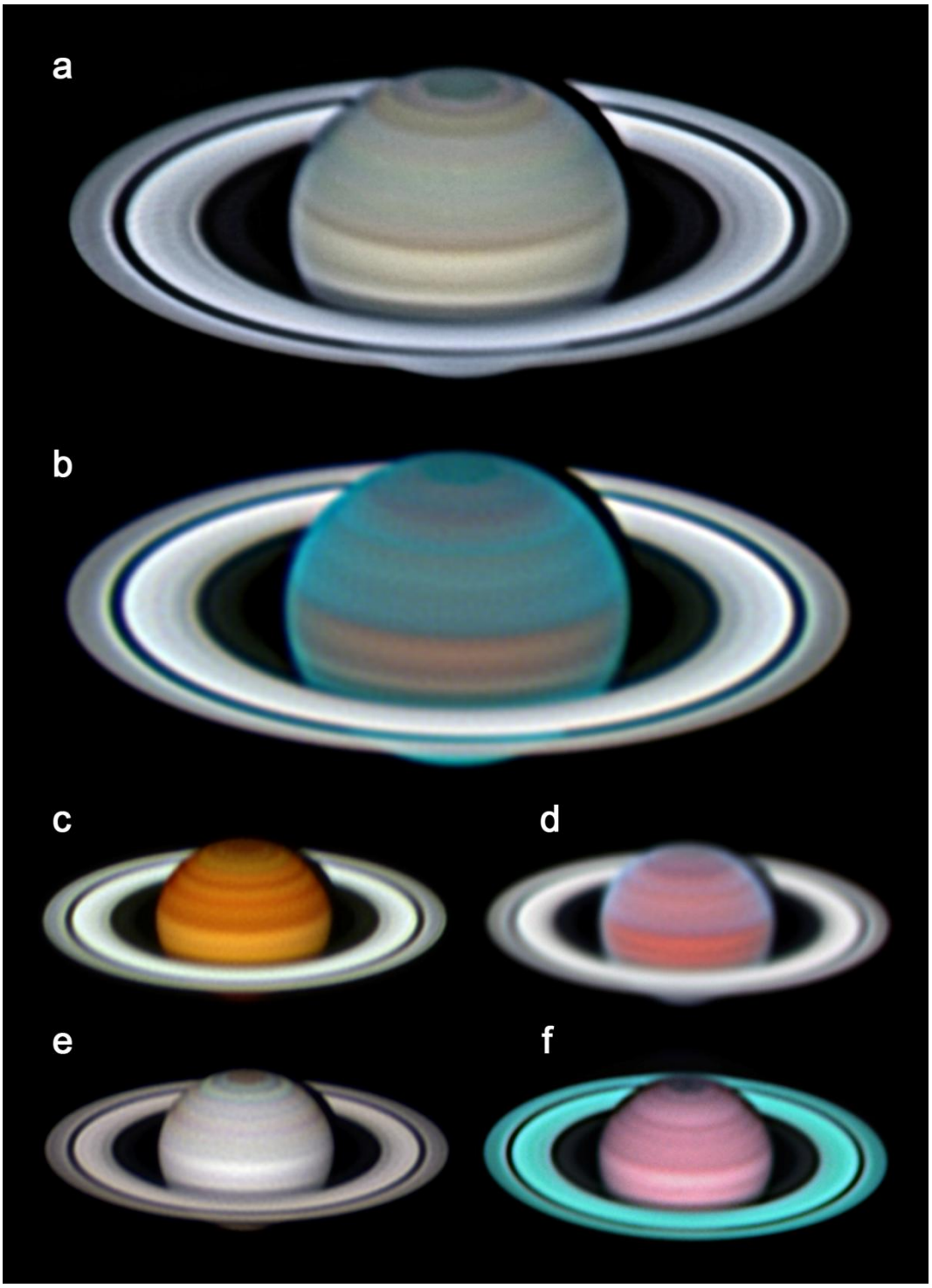

FIG. 20.- *PlanetCam1* observations of Saturn at the 2.2m on 2014-04-06 at maximum magnification (a, b) and minimum magnification on 2014-07-22 (c, d, e) compared with SWIR observations on 2015-05-22 on the 2.2m telescope (f). (a) Color image from R, V, B filters sensitive to the upper clouds. (b) Color image from M2-Vio-U images sensitive to the upper hazes. (c) M1, M2, M3 color image, (d) B-Vio-U color image, (e) C1, C2, C3 color image. (f) H, J, RG1000 SWIR color image. All images have been processed from coregistering a selection of the best frames and using high-pass filters to increase the visibility of atmospheric cloud features Saturn equatorial diameter is 18.3", on panels a and b and 18.6" on panels c, d and e and 18.5" on panel f. North is up and West to the left. Most observations were acquired with Saturn at an approximate elevation of 32º. Frame exposure times vary from 0.01 s to 5 s in different filters.

Imaging of Uranus and Neptune in methane bands in the visible and SWIR channels could allow detecting the major cloud features and tracking their motions to infer winds (Sromovsky et al., 2012; de Pater et al., 2014). Additionally calibrated images can be used to infer the cloud vertical structure in the planet and its long-term changes. Figure 21 shows examples of images of Uranus in both channels.

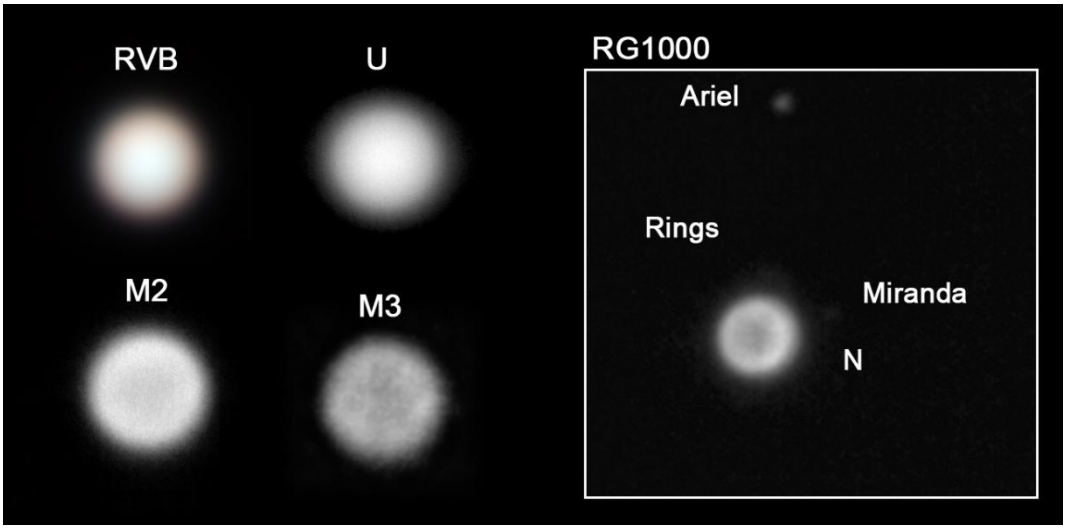

FIG. 21.- Uranus images with *PlanetCam2* at the 2.2m telescope in the visible channel with a variety of filters and in the SWIR channel with the RG1000 filter. All observations were acquired on 2014-12-11 at around 21:10 UT with an elevation angle of ~50º. Uranus size is 3.6" and its apparent magnitude is 5.78. North is to the right. Frame exposure times vary from 0.2 to 2 s in the RG1000 filter and up to 120 s in the M3 filter.

8.3 Outer Solar System bodies

The asteroids Ceres and Vesta, the Galilean satellites, and the satellite Titan are small objects but with a measureable size at high resolution accessible to *PlanetCam*. As an example in Figure 22 we show an image of asteroid Ceres obtained with *PlanetCam1* at CAHA 2.2m using the maximum amplification where its disk of 0.8" can be measured. We also show an image of Jupiter's satellite Ganymede (1.65" in diameter) taken with *PlanetCam1* at the 1.5 m TCS telescope at Teide Observatory. Several surface details can be distinguished that correspond well with those predicted from known surface maps of the satellite. The lowest resolved details have a size of 0.2-0.3 arcsec.

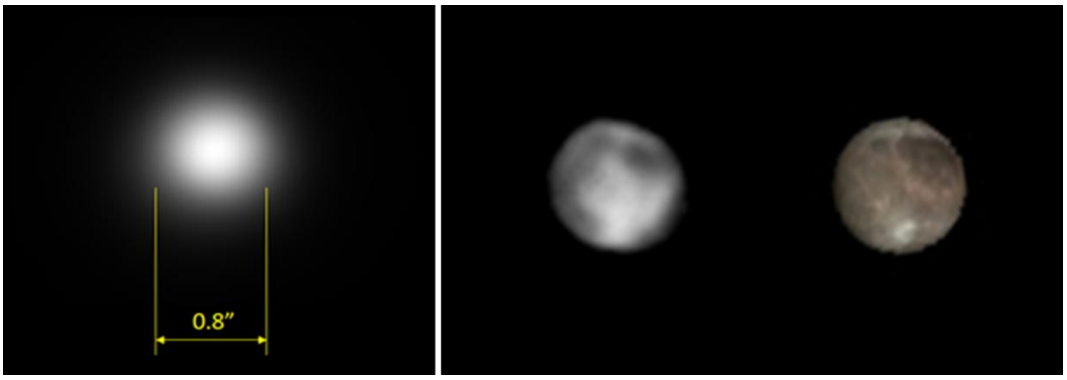

FIG. 22.- Left: The disk of the asteroid Ceres with *PlanetCam1* at the CAHA 2.2m telescope and maximum amplification (barlow x4) obtained on 2014-04-05. Analysis of 1000 frames with exposure times of 0.1 s. Right: *PlanetCam1* observation of Ganymede acquired with the TCS 1.5m telescope on 2013-01-17 at 20:56 UT at high amplification (barlow x2). The image has been processed with Lucy-Richardson deconvolution over a stacking of the best 1% frames from a 300 frames sequence with individual exposure times 0.01 s. Details in Ganymede are compared with the expected details in the surface simulated with the WinJupos software. Ganymede disk is 1.65"

with an apparent magnitude of 4.81 and the observation was run at an elevation angle of 78º. North is up and West to the left. Surface features on Ganymede with a size of 0.15 arcsec can be resolved.

9. APPLICATION TO OTHER ASTRONOMICAL TARGETS

PlanetCam can also be used in studies of other astronomical objects outside the Solar System. We present the results of two astronomical events that require careful temporal resolution. Figure 23 shows a transiting curve for the extrasolar planet WASP 43b in the I band, an ultra-short period (0.81347753 days, Gillon et al., 2012) hot Jupiter orbiting the K7 dwarf star GSC 05490-00141 (Hellier et al, 2011). The host star is a quite red object with a V magnitude of 12.4 and a (V-I) = 1.3 mag. The exoplanet transit has a depth of ~ 0.03 and lasted ~70 minutes at optical wavelengths. The data shown in Figure 23 was obtained for a transit on December 12, 2013, for 60-second individual exposures obtained with *PlanetCam1* attached to the 1.23 m telescope at Calar Alto Observatory. Average scatter is ~2 mmag, showing that under photometric conditions it is possible to reach high precision data.

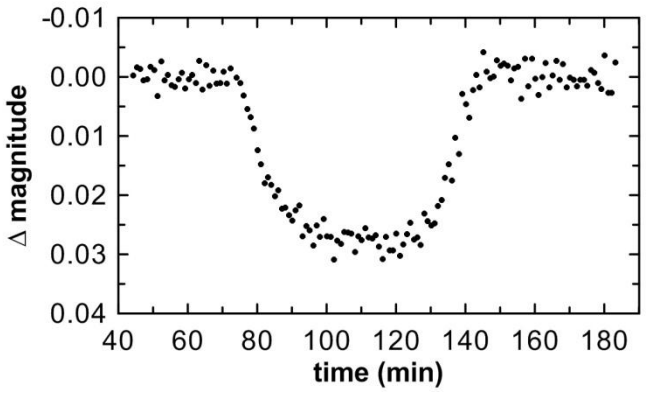

FIG. 23.- WASP-43b transit in the I band captured with *PlanetCam1* attached to the 1.23m telescope at Calar Alto Observatory. Instrumental non-standard magnitudes are given for an arbitrary zero magnitude reference point. Light-curve trend is mostly due to air mass variation between 1.56 and 1.51. Photometric data was extracted using a synthetic aperture procedure.

The second example is the detection and photometric measurements of a Gamma Ray Burst (GRB) event that was observed about one hour after its discovery. The object was GRB 130418A (Gorosabel et al., 2013) and we performed photometry in I band of its optical afterglow using *PlanetCam1* at the 1.23 m CAHA telescope (Figure 24). The analysis of this event is ongoing and here we just show the light curve evolution until de GRB reached a limit magnitude $I \sim 17.5$.

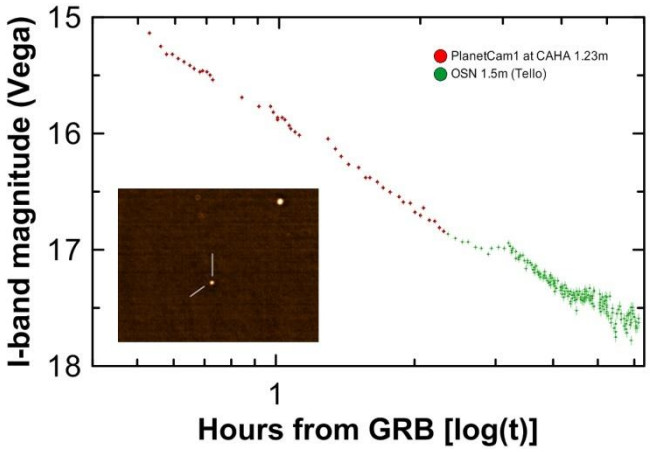

FIG. 24.- Photometric curve of Gamma Ray Burst GRB 130418A in I band detected with *PlanetCam1* at 1.23m CAHA telescope with a total exposure time of 2145.25s (left) and from Tello et al. (2013) at the 1.5m telescope at the Observatory of Sierra Nevada (right), showing a good agreement between both instruments. The inset shows an image of the object.

10. SUMMARY

We present a new and relatively simple low cost astronomical camera *PlanetCam UPV/EHU* for simultaneous imaging of Solar System objects at high spatial resolution in the visible and SWIR spectral ranges (0.38 – 1.7 μm). The camera has been tested in several observation campaigns in a variety of Solar System bodies since June 2012 at Calar Alto Observatory (CAHA) using the 1.23m and 2.2m telescopes, at 1m planetary dedicated telescope at Pic du Midi Observatory, and at the 1.5 m TCS telescope at Teide Observatory, and the camera has also been successfully tested for its use in other astronomical situations. Currently *PlanetCam2* is fully operative at Calar Alto Observatory in Spain.

ACKNOWLEDGEMENTS

This work was supported by the Spanish MICIIN project AYA2012-36666 with FEDER support, Grupos Gobierno Vasco IT-765-13, UPV/EHU UFI11/55 and 'Infraestructura' grants from G. Vasco and UPV/EHU. We thank Drs. Asuncion Illaramendi and Iñaki Bikandi from UPV/EHU for their help and patience during laboratory measurements.

REFERENCES

ANDOR™ Technology, Neo sCMOS, brochure (2012).

Barrado-Izagirre N., J. F. Rojas, R. Hueso, A. Sánchez-Lavega, F. Colas, J.L. Dauvergne, D. Peach, and the IOPW Team (2013). Jupiter's zonal winds and their variability studied with small-size telescopes. Astronomy & Astrophysics, 2013, 554, A74, d.o.i.: 10.1051/0004-6361/201321201.

Belton, M.J.S., and 20 colleagues, 1991. Images from Galileo of the Venus cloud deck. Science 253, 1531–1536.

Fried, D.L. (1965) "Statistics of a geometrical representation of wave-front distortion". J. Opt. Soc. Am., 55, 1427-35.

García-Melendo, E., Legarreta, J., Sánchez-Lavega, A., Hueso, R., Pérez-Hoyos, S., González, J., Gómez-Forrellad, J.M., et al., 2009. The Jovian anticyclone BA: I.Motions and interaction with the GRS from observations and non-linear simulations. Icarus 203, 486–498.

García-Melendo, A. Sánchez-Lavega, J. Legarreta, S. Perez-Hoyos, R. Hueso. "A strong high altitude narro E. w jet detected at Saturn's Equator", Geophysical Research Letters, 37, L22204 (2010).

García-Melendo E., S. Pérez-Hoyos, A. Sánchez-Lavega, R Hueso. Saturn's zonal wind profile in 2004 - 2009 from Cassini ISS images and its long-term variability, Icarus, 215, 62-74 (2011).

Gérard J. C., A. Saglam, G. Piccioni, P. Drossart, C. Cox, S. Erard, R. Hueso, A. Sánchez-Lavega, "The distribution of the O_2 infrared nightglow observed with VIRTIS on board Venus Express", Geophys. Res. Lett. 35 (2008).

Gonzalez R.C., Woods R.E., 2008. Digital Image Processing, third ed. Pearson and Prentice Hall.

Gorosabel J., S. Perez-Hoyos, I. Mendikoa, A. Sanchez-Lavega, R. Hueso, J.F. Rojas, A. de Ugarte Postigo (2013). GCN Circular #14378.

Grant-Smith A. (2010). An examination of Selective Imaging techniques. Master Thesis, MacQuarie University, Sidney, Australia.

Gillon M., Triaud A. H. M. J., Fortney J. J., Demory B.O., Jehin E., Lendl M., Magain P., Kabath P., Queloz D., Alonso R., Anderson D. R., Collier Cameron A., Fumel A., Hebb L., Hellier C., Lanotte A., Maxted P. F. L., Mowlavi N., and Smalley B. (2012). The TRAPPIST survey of southern transiting planets. I. Thirty eclipses of the ultra-short period planet WASP-43 b. Astron. & Astrophys., 542, A4. DOI: 10.1051/0004-6361/201218817.

Hammel H.B., M.H. Wong, J. T. Clarke, I. de Pater, L. N. Fletcher, R. Hueso, K. Noll, G. S. Orton, S. Pérez-Hoyos, A. Sánchez-Lavega, A. A. Simon-Miller and P. A. Yanamandra-Fisher (2010). Jupiter after the 2009 impact: Hubble Space Telescope imaging of the impact-generated debris and its temportal evolution. The Astrophysical Journal Letters, 715, 2, L155.

Hardy, J. W. (2000). "Adaptive optics for astronomical telescopes". Physics today vol. 53, no. 4, p. 69.

Helbert, J., Müller, N., Kostama, P., Marinangeli, L., Piccioni, G., Drossart, P. (2008) Surface brightness variations seen by VIRTIS on Venus Express and implications for the evolution of the Lada Terra region, Venus, Geophysical Research Letters, 35, 11, L11201.

Hellier C., Anderson D. R., Collier Cameron A., Gillon M., Jehin E., Lendl M., Maxted P. F. L., Pepe F., Pollacco D., Queloz D., Ségransan D., Smalley B., Smith A. M. S., Southworth J., Triaud A. H. M. J., Udry S., and West R. G., (2011). WASP-43b: the closest-orbiting hot Jupiter. Astron. & Astrophys., 535, L7. DOI: 10.1051/0004-6361/201117081.

Hormuth F. (2007). AstraLux: High Angular Resolution Astronomywith an Electron Multiplying CCD. Diploma thesis in Physics, Faculty of Physics and Astronomy, University of Heidelberg, Germany.

Hormuth, F., S. Hippler, W. Brandner, K. Wagner, T. Henning (2008). AstraLux: the Calar Alto lucky-imaging camera. Proc. SPIE 7014, Ground-based and Airborne Instrumentation for Astronomy II, 701448 (July 11, 2008); doi:10.1117/12.787384.

Hueso R., A. Sánchez-Lavega, et al. "Morphology and Dynamics of Venus Oxygen Airglow from Venus Express/VIRTIS observations", J. Geophys. Res.-Planets 113, E00B02, (2008).

Hueso, R., J. Legarreta, E. García-Melendo, A. Sánchez-Lavega and S. Pérez-Hoyos (2009). The Jovian anticyclone BA: II. Circulation and interaction with the zonal jets, Icarus, 203, 499-515 (2009).

Hueso, R., A. Wesley, C. Go, S. Pérez-Hoyos, M. H. Wong, L. N. Fletcher, A. Sánchez-Lavega, M. B. E. Boslough, I. de Pater, G. S. Orton, A. A. Simon-Miller, S. G. Djorgovski, M. L. Edwards, H. B. Hammel, J. T. Clarke, K. S. Noll and P. A. Yanamandra-Fishe (2010). First Earth-based detection of a Superbolide on Jupiter. The Astrophysical Journal Letters, 721, 2, L129.

Hueso, R., S. Pérez-Hoyos, A. Sánchez-Lavega, A. Wesley, G. Hall, C. Go, M. Tachikawa, K. Aoki, M. Ichimaru, J. W.

T. Pond, D. G. Korycansky, C. Palotai, G. Chappell, N. Rebeli, J. Harrington, M. Delcroix, M. Wong, I. de Pater, L. N. Fletcher, H. Hammel, G. S. Orton, I. Tabe, J. Watanabe, and J. C. Moreno. (2013). Impact flux on Jupiter: From superbolides to large-scale collisions. Astronomy and Astrophysics, 560, A55 (2013).

Karkoschka, E., Tomasko, M.G., 2010. Methane absorption coefficients for the jovian planets from laboratory, Huygens, and HST data. Icarus 205, 674–694.

Law, N. M., C.D. Mackay, J.E. Baldwin (2005).Lucky Imaging: High Angular Resolution Imaging in the Visible from the Ground. Astronomy & Astrophysics 446, 739 – 745.

Law N. M. (2006). Lucky-imaging: diffraction-limited astronomy from the ground in the visible. Ph.D. Thesis, Cambridge University, Cambridge, UK.

Lelievre, G., Nieto, J.L., Thouvenot, E., Salmon, D., & Llebaria, A. 1988. Very high resolution imaging using sub-pupil apertures, recentering and selection of short exposures. Astronomy and Astrophysics, 200(July), 301–311.

López López R. (2012). Diseño, construcción y desarrollo de un sistema limitado por difracción para telescopios terrestres: FastCam. Ph. D. Thesis, Universidade de Vigo, Vigo, Spain.

Lucy, L. B., 1974. An iterative technique for the rectification of observed distributions. Astronomical Journal, 79, 745–754.

Mousis, O., R. Hueso, J.-P. Beaulieu, S. Bouley, B. Carry, F. Colas, A. Klotz, C. Pellier, J.-M. Petit, P. Rousselot, M. Ali Dib, W. Beisker, M. Birlan, C. Buil, A. Delsanti, E. Frappa, H. B. Hammel, A.-C. Levasseur-Regourd, G. S. Orton, A. Sanchez-Lavega, A. Santerne, P. Tanga, J. Vaubaillon, B. Zanda, D. Baratoux, T. Boehm, V. Boudon, A. Bouquet, L. Buzzi, J.-L. Dauvergne, A. Decock, M. Delcroix, P. Drossart, N. Esseiva, G. Fischer, L. N. Fletcher, S. Foglia, J. M. Gomez-Forrellad, J. Guarro-Flo, D. Herald, F. Kugel, J.-P. Lebreton, J. Lecacheux, A. Leroy, L. Maquet, G. Masi, A. Maury, F. Meyer, S. Pérez-Hoyos, A. S. Rajpurohit, C. Rinner, J. H. Rogers, F. Roques, R. W. Schmude, Jr., B. Sicardy, B. Tregon, M. Vanhuysse, A. Wesley, T. Widemann (2014). Instrumental Methods for Professional and Amateur Collaborations in Planetary Astronomy. Experimental Astronomy, 38, 91-191 (2014).

Ordoñez-Etxebarria I., R. Hueso, A. Sánchez-Lavega, S. Pérez-Hoyos. “Spatial distribution of Jovian clouds, hazes and colors from Cassini ISS multi-spectral images”, Icarus (submitted, 2015).

Parker, D.C., Beish, J.D., Troiani, D.M., Joyce, D.P., Hernandez, C.E.: Telescopic observations of Mars, 1996-1997: Results of the Marswatch program. Icarus 138, 3–19 (1999).

Peralta J., R. Hueso and A. Sánchez-Lavega (2007). A reanalysis of Venus winds at two cloud levels from Galileo SSI images. Icarus, 190, 469-477 (2007).

Pérez-Hoyos S., A. Sánchez-Lavega, R.G. French, J.F. Rojas. Saturn’s cloud structure and temporal evolution from ten years of Hubble Space Telescope images (1994–2003). Icarus 176 (2005) 155–174.

Pérez-Hoyos, S., Sánchez-Lavega, A., Hueso, R., García-Melendo, E., Legarreta, J., 2009. The Jovian anticyclone BA: III. Aerosol properties and color change. Icarus 203, 516–530.

Pérez-Hoyos S., J.F. Sanz-Requena, N. Barrado-Izagirre, J.F. Rojas, A. Sánchez-Lavega (2012). The 2009-10 Fade of Jupiter's South Equatorial Belt: vertical cloud structure models and zonal winds from visible imaging. Icarus, 217, 256-271 (2012).

Qiu, P., Y.N. Mao, X.M. Lu, E. Xiang, X.J. Jian (2012). Evaluation of a scientific CMOS camera for astronomical observations. Research in Astronomy and Astrophysics, 13, 615, doi:10.1088/1674-4527/13/5/012.

Richardson, W. H., 1972. Bayesian-Based Iterative Method of Image Restoration. JOSA, 62, 55-59.

Sánchez-Lavega, A., R. Hueso, G. Piccioni, P. Drossart, J. Peralta, S. Pérez-Hoyos, C. F. Wilson, F. W. Taylor, K. H. Baines, D. Luz, S. Erard and S. Lebonnois (2008). Variable winds on Venus mapped in three dimensions. Geophys. Res. Lett., 35, L13204, doi:10.1029/2008GL033817, (2008).

Sánchez-Lavega A., G. S. Orton, R. Hueso, E. García-Melendo, S. Pérez-Hoyos, A. Simon-Miller, J. F. Rojas, J. M. Gomez, P. Yanamandra-Fisher, L. Fletcher, J. Joels, J. Kemerer, J. Hora, E. Karkoschka, I. de Pater, M. H. Wong, P. S. Marcus, N. Pinilla-Alonso, F. Carvalho, C. Go, D. Parker, M. Salway, M. Valimberti, A. Wesley and Z. Pujic (2008). Depth of a strong jovian jet from a planetary-scale disturbance driven by storms, Nature, 451, 437-440.

Sánchez-Lavega A., A. Wesley, G. Orton, R. Hueso, S. Perez-Hoyos, L. N. Fletcher, P. Yanamandra-Fisher, J. Legarreta, I. de Pater, H. Hammel, A. Simon-Miller, J. M. Gomez-Forrellad, J. L. Ortiz, E. García-Melendo, R. C. Puetter and P. Chodas (2010). The impact of a large object on Jupiter in 2009 July. The Astrophysical Journal Letters, 715, 2, L150.

Sánchez-Lavega A., T. del Río-Gaztelurrutia, R. Hueso, J. M. Gomez-Forrellad, J. F. Sanz-Requena, J. Legarreta, E. García-Melendo, F. Colas, J. Lecacheux, L. N. Fletcher, D. Barrado-Navascués, D. Parker & the International Outer Planet Watch Team, T. Akutsu, T. Barry, J. Beltran, S. Buda, B. Combs, F. Carvalho, P. Casquinha, M. Delcroix, S. Ghomizadeh, C. Go, J. Hotershall, T. Ikemura, G. Jolly, A. Kazemoto, T. Kumamori, M. Lecompte, P. Maxson, F. J. Melillo, D. P. Milika, E. Morales, D. Peach, J. Phillips, J. J. Poupeau, J. Sussenbach, G. Walker, S. Walker, T. Tranter, A. Wesley, T. Wilson & K. Yunoki for The International Outer Planet Watch (IOPW) Team (2011). Deep winds beneath Saturn's upper clouds from a seasonal long-lived planetary-scale storm. Nature 475, 71-74; doi:10.1038/nature10203.

Sánchez-Lavega, A., (2011). An Introduction to Planetary Atmospheres, Taylor & Francis (CRC), Florida.

Sánchez-Lavega A., J. F. Rojas, R. Hueso, S. Pérez-Hoyos, L. de Bilbao, G. Murga, J. Ariño (2012). PlanetCam UPV/EHU: A simultaneous visible and near infrared lucky-imaging camera to study Solar System objects. Proc. of SPIE Vol. 8446 84467X-1.

Sánchez-Lavega A., J. Legarreta, E. García-Melendo, R. Hueso,S. Pérez-Hoyos, J. M. Gómez-Forrellad, L.N. Fletcher, G. S. Orton, A. S. Miller, N. Chanover, P. Irwin, P. Tanga, M. Cecconi, and the IOPW and ALPO Japan contributors. Colors of Jupiter's large anticyclones and the interaction of a Tropical Red Oval with the Great Red Spot in 2008. J. Geophys. Res., 118, 1-21 (2013).

Sánchez-Lavega A., A. García Muñoz, E. García-Melendo, S. Pérez-Hoyos, J. M. Gómez-Forrellad, C. Pellier, M. Delcroix, M. A. López-Valverde, F. González-Galindo , W. Jaeschke, D. Parker, J. Phillips, and D. Peach. An extremely high altitude plume seen at Mars morning terminator, Nature, 518, 525- 528 (2015).

Sanz-Requena J.F., S. Pérez-Hoyos, A. Sánchez-Lavega, T. del Río-Gaztelurrutia, D. Barrado-Navascués, F. Colas, J. Lecacheux and D. Parker (2012). Cloud structure of Saturn's Storm from ground-based visual imaging. Icarus, 219, 142-149.

Simon-Miller A.A., D. Banfield and P. J. Gierasch (2001a), An HST study of Jovian chromophores, Icarus, 149, 94–106.

Simon-Miller, A.A., D. Banfield, and P. J. Gierasch, (2001b), Color and the vertical structure in Jupiter's belts, zones, and weather systems, Icarus 154, 459–474.

Simon A. A., Miller, R. W. Carlson, A. Sanchez-Lavega. Spectral Comparison and Stability of Red Regions on Jupiter, J. Geophys. Res. (in press, 2015).

Smith W. J., Modern Optical Engineering, McGraw-Hill, Third edition (2000).

Souchay J., Feissel-Vernier M. (eds.) (2006), The International Celestial Reference System and Frame. IERS Technical Note, N. 34, Verlag des Bundesamts für Kartographie und Geodäsie, Frankfurt am Main.

Sromovsky L.A., H.B. Hammel, I. de Pater, P.M. Fry, K.A. Rages, M.R. Showalter, W.J. Merline, P. Tamblyn, C. Neyman, J.-L. Margot, J. Fang, F. Colas, J.-L. Dauvergne, J.M. Gomez-Forrellad, R. Hueso, A. Sanchez-Lavega, Thomas Stallard (2012). Episodic bright and dark spots on Uranus. Icarus, 220, 6-22 (2012).

Strycker P. D., N. J. Chanover, A. A. Simon-Miller, D. Banfield, and P. J. Gierasch (2011).Jovian chromophore characteristics from multispectral HST images. Icarus, 215, 552–583.

Tello J.C., Sanchez-Ramirez R., Gorosabel J., Aceituno F. and Castro-Tirado A. (2013), GRB130418A: OSN 1.5m fading afterglow detection. GCN # 14385.

Titov, D. V., W. J. Markiewicz, N. I. Ignatiev, L. Song, S. S. Limay, A. Sanchez-Lavega, M. Almeida, T. Roatsch, K. D. Matz, F. Scholten, D. Crisp, L. W. Esposito, S. F. Hviid, R. Jaumann, H. U. Kelle, R. Moissl, "Morphology of the cloud tops as observed by the Venus Express Monitoring Camera", Icarus, 217, 682-701 (2012).

Travis, L.D., 1978. Nature of the atmospheric dynamics on Venus from power spectrum analysis of Mariner 10 images. J. Atmos. Sci. 35, 1584–1595.

Washington Visual Double Star Catalog (WDS), 2014 http://ad.usno.navy.mil/proj/WDS/

West, R. A. and M. G. Tomasko, Spatially resolved methane band photometry of Jupiter. III - Cloud vertical structures for several axisymmetric bands and the Great Red Spot, Icarus 41, 278–292, 1980.

West, R.A., 1982. Spatially resolved methane band photometry of Saturn: I. Absolute reflectivity and center-to-limb variations in the 6190-, 7250-, and 8900-A bands. Icarus 51, 51–64.

West, R.A., 1983. Spatially resolved methane band photometry of Saturn: II. Cloud structure models at four latitudes. Icarus 53, 301–309.

West, R.A., Sato, M., Hart, H., Lane, A.L., Hord, C.W., Simmons, K.E., Esposito, L.W., Coffeen, D.L., Pomphrey, R.B., 1983. Photometry and polarimetry of Saturn at 2640 and 7500 A. J. Geophys. Res. 88, 8679–8697 (1969).